The Neutron Detection Efficiency Measurements
Of a 10 inch NE213 Scintillator

by

Abdulla Abdulaziz Al-Sunaidi

A Thesis Presented to the

FACULTY OF THE COLLEGE OF GRADUATE STUDIES

KING FAHD UNIVERSITY OF PETROLEUM & MINERALS

DHAHRAN, SAUDI ARABIA

In Partial Fulfillment of the
Requirements for the Degree of

MASTER OF SCIENCE

In

PHYSICS

January, 1992

INFORMATION TO USERS

This manuscript has been reproduced from the microfilm master. UMI films the text directly from the original or copy submitted. Thus, some thesis and dissertation copies are in typewriter face, while others may be from any type of computer printer.

The quality of this reproduction is dependent upon the quality of the copy submitted. Broken or indistinct print, colored or poor quality illustrations and photographs, print bleedthrough, substandard margins, and improper alignment can adversely affect reproduction.

In the unlikely event that the author did not send UMI a complete manuscript and there are missing pages, these will be noted. Also, if unauthorized copyright material had to be removed, a note will indicate the deletion.

Oversize materials (e.g., maps, drawings, charts) are reproduced by sectioning the original, beginning at the upper left-hand corner and continuing from left to right in equal sections with small overlaps. Each original is also photographed in one exposure and is included in reduced form at the back of the book.

Photographs included in the original manuscript have been reproduced xerographically in this copy. Higher quality 6" x 9" black and white photographic prints are available for any photographs or illustrations appearing in this copy for an additional charge. Contact UMI directly to order.

U·M·I

University Microfilms International
A Bell & Howell Information Company
300 North Zeeb Road, Ann Arbor, MI 48106-1346 USA
313/761-4700 800/521-0600

Order Number 1355323

The neutron detection efficiency measurements of a 10 inch NE213 scintillator

Al-Sunaidi, Abdulla Abdulaziz, M.S.

King Fahd University of Petroleum and Minerals (Saudi Arabia), 1992

U·M·I
300 N. Zeeb Rd.
Ann Arbor, MI 48106

THE NEUTRON DETECTION EFFICIENCY MEASUREMENTS OF A 10 INCH NE213 SCINTILLATOR

BY

ABDULLA ABDULAZIZ AL-SUNAIDI

A Thesis Presented to the
FACULTY OF THE COLLEGE OF GRADUATE STUDIES
KING FAHD UNIVERSITY OF PETROLEUM & MINERALS
DHAHRAN, SAUDI ARABIA

In Partial Fulfillment of the
Requirements for the Degree of

MASTER OF SCIENCE
In
PHYSICS

JANUARY 1992

KING FAHD UNIVERSITY OF PETROLEUM & MINERALS

DHAHRAN, SAUDI ARABIA

COLLEGE OF GRADUATE STUDIES

REPORT ON "FINAL COMPREHENSIVE EXAMINATION" FOR MASTER'S DEGREE

ABDULLA ABDULAZIZ AL-SUNAIDI (STUDENT ID#830849) has successfully defended his thesis entitled"THE NEUTRON DETECTION EFFICIENCY MEASUREMENTS OF A 10 INCH NE213 SCINTILLATOR" in a Final Comprehensive Examination for completion of the Master's Degree. As his thesis committee, we certify that we have read the thesis and approved it, and we hereby recommend its acceptance by the Dean, College of Graduate Studies.

Dean, College of Graduate Studies
Dr. Ala Al-Rabeh

Date: 22 1 92

Department Chairman
Dr. A. D. Al-Haidari

Date: 15/1/92

Thesis Committee:

Dr. H. A. Al-Juwair: ______________ (Advisor)

Dr. A. A. Naqvi : ______________ (Co-Advisor)

Dr. H. A. Mavromatis : Harry V Mavromatis (Member)

Dr. M. A. Salim : ______________ (Member)

ACKNOWLEDGMENT

I would like to express my warm thanks to my thesis committee, Dr. H. Al-Juwair and Dr. A. A. Naqvi for their considerable assistance and guidance during the experimental work, and Dr. H. A. Mavromatis and Dr. M. Salim for their valuable suggestions.

I wish also to thank the operating groups in the Energy Research Laboratory, especially the Neutron Generator Group and the Health Physics Group for appreciable cooperation. I owe a special debt to Dr. R. Abdel-Aal who put too much effort to run the VAX computer.

Finally, I wish to thank King Fahd University of Petroleum and Minerals for support of this research. In particular, I gratefully acknowledge the Physics Department and the Energy Research Laboratory for putting all their facilities available to me to complete this research.

TABLE OF CONTENTS

page

LIST OF TABLES vi

LIST OF FIGURES vii

ABSTRACT ix

CHAPTER 1 INTRODUCTION 1
- 1.1 NE213 Scintillators Neutron Detection Efficiency 1
- 1.2 NE213 Scintillators Response Function 6
- 1.3 Present Status of the Problem 10

CHAPTER 2 DETECTOR MODIFICATION 12

CHAPTER 3 PERFORMANCE TESTS 23
- 3.1 Energy Resolution Test 24
  - *3.1.1 Experimental Procedure* 25
  - *3.1.2 Data Acquisition System* 28
  - *3.1.3 Results and Analysis* 31
- 3.2 Time Resolution Test 41
  - *3.2.1 Experimental Procedure* 42
  - *3.2.2 Results and Analysis* 48

3.3 Pulse Shape Discrimination Test .. 53
3.3.1 Experimental Procedure 54
3.3.2 Results and Analysis 59

CHAPTER 4 NEUTRON DETECTION EFFICIENCY MEASUREMENTS 62
4.1 Experimental Technique 62
4.1.1 General Considerations 62
4.1.2 Equipment 64
4.1.3 Three-Parameter Data Aquisition 65
4.1.4 Neutron Source 66
4.1.5 Procedure 70
4.2 Data Analysis 73
4.2.1 Analysis of the Time-of-Flight Spectra 77
4.2.1a Response Function 79
4.2.1b Efficiency Measurements 89

CHAPTER 5 SUMMARY AND CONCLUSION 92

APPENDIX A AQUISITION & ANALYSIS CODES ... 96

NOMENCLATURE 105

REFERENCES 106

LIST OF TABLES

Table Page

2.1 Properties of NE213 scintillators 13

3.1 Standard gamma ray sources 27
3.2 Energies of backscattered electrons 30
3.3 Effect of LG on energy resolution 32
3.4 Published data on energy resolution 37
3.5 Energy resolution parameters 39
3.6 Effect of energy bias on time resolution 49
3.7 Effect of LG on PSD parameters 60

4.1 Response function data 86

5.1 Effect of LG on the Detector Performance 93

LIST OF FIGURES

Figure Page

1.1 n-p and n-C total cross sections 5
1.2 Angular distribution of Compton electrons 8

2.1 Assembly of the NE213 scintillator 14
2.2 Schematic diagram of the 10" scintillator 16
2.3 The scintillator in direct coupling to the PM tube .. 18
2.4 First stage in deassembling the detector 19
2.5 Coupling of the painted LG to the scintillator 20
2.6 Mounting the PM tube 21
2.7 The 10" scintillator in the final stage 22

3.1 Electronics used in the energy resolution test 29
3.2 Compton edge & coincidence peak before incorporating the LG 33
3.3 Compton edge & coincidence peak after incorporating the LG 34
3.4 Polynomial fit to the coincidence peak 35
3.5 Energy resolution against electron energy 40
3.6 Decay scheme of the ^{60}Co gamma source 43
3.7 Electronics used in the time resolution 46
3.8 A typical time calibration spectrum 47
3.9 Dependence of time resolution on energy bias 50
3.10 A typical time coincidence peak 51
3.11 Electronics used in the PSD test 55
3.12 A typical PSD spectrum 57
3.13 Effect of count rate on PSD performance 58

4.1 Electronics used in the TOF measurements 67
4.2 Three-parameter data acquisition system 68
4.3 Time correlation of the TOF, PSD and pulse height signals 69
4.4 ^{252}Cf source neutron energy spectrum 72
4.5 A typical TOF spectrum 74
4.6 A typical PSD spectrum from ^{252}Cf source 75
4.7 A pulse-height spectrum from the ^{252}Cf source 76
4.8 Relation between proton energy and the TOF channel number 78
4.9a The added TOF spectrum 81
4.9b The TOF spectrum after setting the PSD gates 82
4.9c Energy gates on the neutron TOF spectra 83
4.9d The proton recoil edge 84
4.10 Calibration with gamma sources 85
4.11 Response curve 87
4.12 Efficiency curves 91

ABSTRACT

NAME : ABDULLA ABDULAZIZ AL-SUNAIDI

TITLE : THE NEUTRON DETECTION EFFICIENCY MEASUREMENTS OF A 10 INCH NE213 SCINTILLATOR USING ^{252}Cf SOURCE

MAJOR : PHYSICS

DATE : JANUARY 1992

A 10 inch NE213 scintillator in direct coupling to a 5 inch photomultiplier was modified by incorporating a light guide between the scintillation cell and the photomultiplier. Three tests were carried out to see the effect of the light guide on the performance of the detector. Results of the first test, which agreed with published data, showed an improvement in the detector energy resolution of about 50%. In the time resolution test, an improvement of about 30% was acheived. Finally, no noticeable change in the neutron-gamma discrimination at operating biases was recorded. After this improvement in the performance of the detector, the response function and the neutron detection efficiency of the modified detector were studied utilizing the Time-of-Flight technique and using a ^{252}Cf fission neutron source.

MASTER OF SCIENCE DEGREE
KING FAHD UNIVERSITY OF PETROLEUM & MINERALS
DHAHRAN, SAUDI ARABIA
January 1992

خلاصة الرسالة

العنوان : قياس كفاءة كشف النيوترونات لومّاض من النوع إن إي ٢١٣

الإسم : عبدالله عبدالعزيز حسين السنيدي

التخصص : فيزياء

التاريخ : رجب ١٤١٢هـ

في هذا البحث، جرى تعديل التصميم الأصلي لكاشف نيوترونات ومّاض من النوع إن إي٢١٣ بقطر ١٠ إنش موصل مباشرةً بمضاعف ضوئي بقطر ٥ إنش وذلك بإدخال قائد ضوئي مخروطي بين الومّاض و المضاعف الضوئي. وقد أجريت ثلاثة إختبارات لدراسة تأثير القائد الضّوئي على أداء الكاشف. نتائج الإختبار الأول والتي تطابقت مع النتائج المنشورة سابقاً أظهرت تحسناً بمقدار٥٠٪ في قدرة الكاشف على تمييز الطاقه. أمّا في إختبارقدرة التمييزالزمني للكاشف فقد سجل تحسنٌ بمقدار ٣٠٪. أخيراً لوحظ تراجع محدود في قدرة الكاشف على التفريق بين النيوترونات و أشعة غاما يتناقص كلّما زادت مقادير الطّاقه. بعد هذا التحسن العام في أداء الكاشف تمّ إيجاد دالّة إستجابة الكاشف للنيوترونات و قياس كفاءة الكاشف بإستخدام طريقة " زمن الإنتقال " وإستخدام عنصر الكاليفورنيوم(٢٥٢) المشع كمصدر للنيوترونات.

درجة الماجستير في العلوم
جامعة الملك فهد للبترول و المعادن
الظهران- المملكة العربية السعودية
رجب ١٤١٢ هـ

CHAPTER ONE

INTRODUCTION

One of the most important quantities in the study of the structure of nuclei is the scattering cross section. Experiments done in this field usually use nucleons as the bombarding particles. Therefore, the detectors used in such experiments should show good response to these particles. NE213 liquid scintillation detectors are preferred for fast neutron spectroscopy for their good response to neutrons, good energy resolution, good time resolution and good neutron-gamma discrimination [1]. However, these detectors are not 100% efficient for the detection of neutrons. Therefore, before cross section experiments are done, calibration of these detectors in terms of their neutron detection efficiency must be carried out.

1.1 NE213 SCINTILLATOR NEUTRON DETECTION EFFICIENCY

The neutron detection efficiency η is an intrinsic property of the detector used. It is a quantity relating the fraction of pulses recorded by the detector with energy E, to the number of the neutrons incident on the detector, or

$$\eta(E) = \frac{\text{number of detected neutrons}}{\text{number of incident neutrons}}$$

The fact that neutrons are neutral, means that the detection of the neutrons is possible after a number of interactions with the scintillator material. The possibility of not being detected, results in making the detector having a reduced efficiency.

There are several factors that have direct effects on the efficiency measurement. Efficiency is always measured with respect to some threshold level, or energy bias. This bias is set in order to suppress noise inherent by electronics and to get rid of background neutrons. Neutrons with energies less than this bias are not counted, and therefore the efficiency drops to zero for energies below this bias. As the energy bias increases, the efficiency decreases. Also with increasing the neutron energy the efficiency decrease. This happens because as the neutron energy increases, the probability of interaction with the scintillator material decreases. However, to increase this probability, the scintillator volume is enlarged. Since small diameter photomultipliers have better quantum efficiency than large ones, and commercial photomultipliers have limited sizes, people have used conical light guides to couple scintillators of large sizes to photomultipliers with smaller sizes [2].

Another factor that affects the efficiency of a scintillation detector is the concentration of hydrogen nuclei with respect to other nuclei. Increasing the number of hydrogen nuclei enhances the n-p scattering cross section which improves the efficiency. This is one of the main things that made the NE213 liquid scintillators a good neutron detector. The ratio of hydrogen nuclei to carbon nuclei in this scintillator is 1.2 [3].

Several techniques on the experimental measurement of the neutron detection efficiency of detectors were reported. In these techniques, either accelerator based neutron sources or fission neutron sources are used. Accelerator based sources produce monoenergetic neutrons either directly using deuterium and tritium targets or indirectly from the scattering with hydrocarbon targets. The resulting neutrons will have energies dependent on the scattering angle. Reactions such as D(d,n)^{3}He, T(d,n)^{4}He, and T(p,n)^{3}He, are are widely used in efficiency measurements. In the associated particle technique[4], for example, the helium particles are detected in a solid state detector with 100% efficiency in a fixed solid angle, while the neutrons are counted in a scintillator in coincidence with the helium particles. The ratio of the number of neutrons to helium nuclei gives the relative efficiency of the scintillator. Efficiency was also measured by point-by-point comparison of the total number of neutrons detected by a scintillator with those detected by a calibrated detector, whose efficiency has already been measured[5]. In this case the efficiency is the ratio of neutrons counted by the detector under study to those counted by the calibrated detector multiplied by the efficiency of the calibrated detector. Other techniques, such as the differential method and the comparison of the yields of an angular distribution measurements with the differential cross sections are also sometimes employed[6].

Accelerator based sources and hydrogenous targets are not always available for efficiency measurements. Therefore, spontaneous neutrons emitted from fission isotopes like ^{252}Cf are sometimes used instead[7]. The disadvantage of these sources is that they emit neutrons with continuous, limited, energy spectrum. However they have some advantages over the accelerator based neutron sources. They can be manufactured in small sizes, and the emitted neutrons have a well defined distribution. Several distributions, such as the Watt distribution[8] and the Maxwellian distribution[9] based on the evaporation theory[10] are believed to fit the experimentally determined neutron spectrum. Efficiency measurements using these sources are usually done by comparing the number of neutrons counted by the scintillator under study at a known energy with that extracted from the standard spectrum. Most of the efficiency measurements made with the two sources; accelerator based sources and the ^{252}Cf source utilize the Time-of-Flight technique[11], to measure the neutron energy.

Since efficiency measurements can not be carried out in very small energy steps, and therefor the measured points do not cover all the energy range of interest, the need for computer calculation that fit the experimental data was demanding. Several codes were written for this purpose, but those based on the Monte Carlo method are widely used[12,13]. In this method, the statistical behavior of a neutron incident on the scintillator is simulated. This requires information about the different probabilities of the interaction of the neutron with the scintillation material. Since the NE213 scintillator contains hydrogen and carbon nuclei, a precise knowledge of the n-p and n-C scattering cross sections is important. These reactions were studied thoroughly[14,15,16]. As can be seen in figures 1.1, the n-p cross section dominates at low neutron energies. At neutron energies more than 8 MeV, however, the contribution from the n-C reaction to the efficiency curve is pronounced. Cross sections from other reactions like carbon break-up should also be supplied. Another important information to be as an

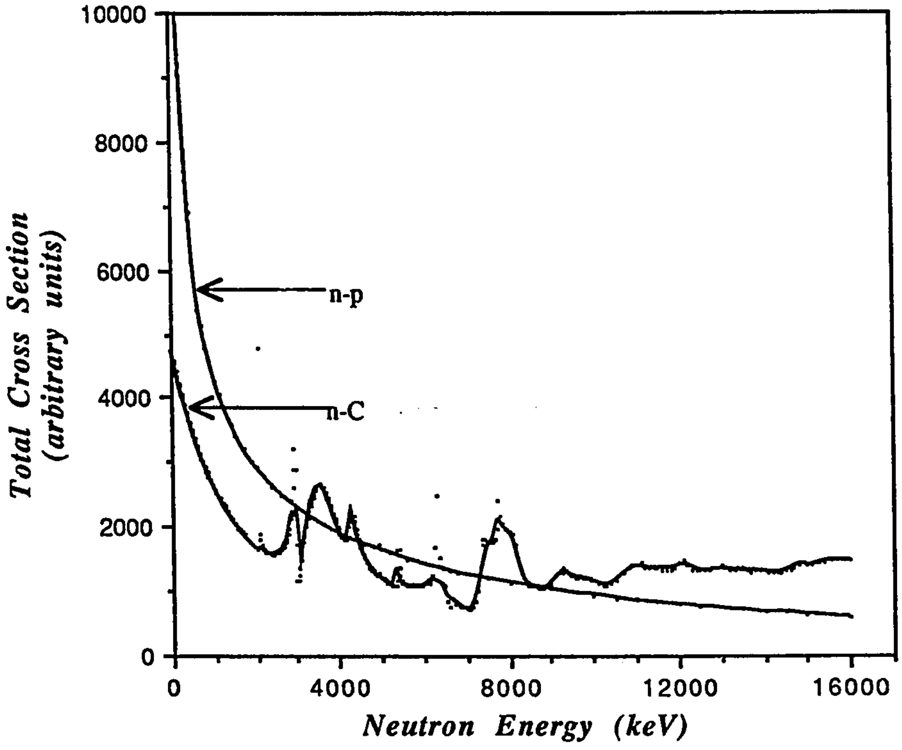

Fig.1.1. The n-p and the n-C total cross sections as a function of neutron energy.

input in the Monte Carlo calculation is the response function. This function predicts the amount of light produced when a particle of a specific energy interacts with the material of the scintillator. This function is usually measured experimentally before the efficiency measurement is done.

1.2. RESPONSE FUNCTION OF NE213 SCINTILLATORS

Scintillators respond indirectly to neutral radiations e.g. gamma rays and neutrons , through recoil charged particles. The charged particles produced excite the molecules of the scintillation material, and a fluorescent light is produced from the de-excitation. The amount of particle energy converted into light is dependent on the mechanism in which the radiation interacts with the scintillation material.

In organic scintillators where the Z value is small, Compton scattering is the most probable process by which gamma rays of energy range of a few MeV, interact. This process results in a recoil electron which has a large fraction of the incident gamma ray energy, depending on the angle of scattering. The dependence on the scattering angle is given by

$$E_e = \frac{E_\gamma^2(1-\cos\vartheta)}{m_o c^2 + E_\gamma(1-\cos\vartheta)}$$

The recoil electron,Compton electrons, will have a maximum energy at a head-on-collision, given by

$$E_C = \frac{2E_\gamma^2}{m_o c^2 + 2E_\gamma}$$

Fig.1.2, shows the distribution for different incident gamma ray energies, as given by the Klein-Nishina formula[3]. The intensity of Compton electrons decreases with increasing energy. The sharp edge corresponds to Compton electrons of maximum energy.

Neutrons, being heavy, uncharged particles, penetrate the electron cloud and collide with nuclei. For low-Z value, which is the case in the NE213 scintillator, the most probable interaction is the scattering of neutrons with nuclei resulting in recoil nuclei. The energy transferred to a recoil nucleus having mass number A is given by

$$E_R = \frac{4AE_n}{(1+A)^2}\cos^2\alpha$$

where α is the angle of recoil. At $\alpha = 0$, the energy transferred is maximum. Since hydrogen (A = 1) is the main constituent of NE213 scintillators, the n-p scattering is most probable. In a head-on-collision, the neutron imparts all its energy to the proton. At energies below 10 MeV, the n-p scattering is isotropic and the energy spectrum of recoil protons has a rectangular shaped distribution[17]. The sharp cut in the distribution spectrum in this case correspond to the incident neutron energy.

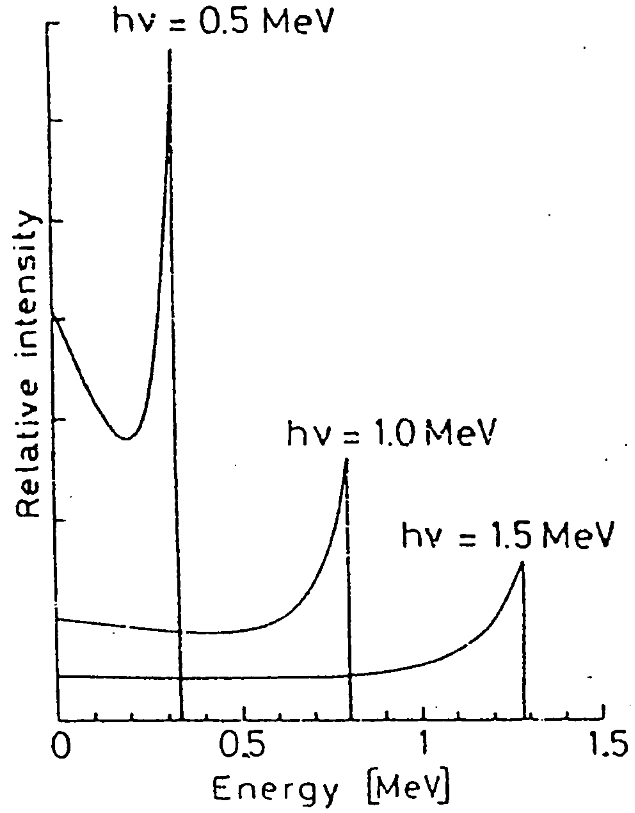

Fig.1.2. The distribution of Compton electrons as predicted by the Klein-Nishina formula for the gamma ray energies, 0.5, 1.0 and 1.5 MeV.

The light output from the two processes was studied thoroughly. It was found that electrons produce more light compared to protons when stopped in organic scintillators[18]. Birks[19] has expressed the differential light output from scintillators in terms of the specific energy loss, dE/dx, for the charged particles. Later studies modified Birks formula by adding additional parameters. The final formula for the light output in integral form with respect to particle energy[20] is

$$L(E) = \eta\int_0^E d\varepsilon\left[1 + kB(dE/dx) + c(dE/dx)^2\right]^{-1}$$

where η is the detector efficiency, dE/dx is the specific energy loss and k,B and C are constants. For electrons, the light output is almost linear for electron energies $E_e \geq 40 MeV$ [21] which means that $dE/dx \approx 0$ and the above equation reduces to

$$L_e(E) \approx \eta E + L_o$$

Scintillators, however, show non-linear response to protons[21]. For this reason, response function is always expressed as a correlation between the proton energy and the electron energy with the same light output.

Experimental determination of the response function is usually done by analyzing the pulse-height spectra. For electrons, Compton edge represent the pulse-height spectrum. Since theoretical calculations do not take into account the limited resolution of the scintillator, the edge produced experimentally does not show a sharp cut as in fig1.2. This diffuseness is related to the volume of conventionally taken as the position of the half-height the Compton edge,L_h[1]. For protons, in addition to resolution problems, the n-C scattering also contribute to the diffuseness of the proton pulse-height spectrum. Therefore, the same convention is used as in the diffused Compton edge. The response function relates these two positions of the proton energy and the electron energy if they produce the same light output.

1.3. PRESENT STATUS OF THE PROBLEM

Scintillators having large diameter are preferred in neutron experiments where the count rate is low. It is believed that they also have better efficiency. However, the light collection process deteriorates with increasing size of the scintillator. Therefore most of the published efficiency data are for scintillators with diameters smaller than 10 inch (250 mm)[6]. Mubarakmand and Anwar[22], reported efficiency measurement of a 10"diam.x1"thick NE213 scintillator coupled with two photomultipliers. They used accelerator based neutron source for their measurement. Bottger et al.[23] have measured the efficiency of a 10" diam.x 2" thick NE213 scintillator coupled to a smaller photomultiplier via a light guide. They also used accelerator based neutron source.

In this project, a systematic study of the neutron detection efficiency of a 10"(250 mm)diam.x 2"(50 mm) thick NE213 liquid scintillator was carried out. This detector is to be used by the Energy Research Laboratory (ERL) at King Fahd

University of Petroleum and Minerals (KFUPM) in neutron scattering experiments. It was originally designed for timing experiments and has bad energy resolution. Therefore, the measurement was performed in two stages. First, the energy resolution and the time resolution of the scintillator were improved by incorporating a light guide between the scintillator and the photomultiplier. Second, the response function and the efficiency of the scintillator were measured with a ^{252}Cf neutron source and utilizing the Time-of-Flight technique.

CHAPTER TWO

DETECTOR MODIFICATION

The detector under study was manufactured by Nuclear Enterprises Ltd. It consists of two parts: a NE213 liquid scintillator and a photomultiplier. The NE213 scintillator consists of xylene, activators, and POPOP as a wavelength shifter. Naphthalene is added to enhance the slow components of light emission [10]. Other properties of the NE213 scintillator are given in table 2.1. The NE213 scintillator fills a cylindrical aluminium housing which is 10" (250 mm) in diameter and 2" (50 mm) thick. The wall thickness of the Al-cell is 2 mm. It is painted from the inside with a white titanium dioxide reflector. For optimum light output, the cell was deoxygenated. One side of the cell has a glass window which allows the optical coupling to the photomultiplier. This window was covered with Al-reflector with a central hole of 130 mm. The detector was coupled to a fast 130 mm photomultiplier tube (PM tube) model 9823B through the hole in front of the glass window. The PM tube converts the weak light signal into a detectable electrical pulse. It has a rise time of 2.7 nsec and a linear focussed structure of 14 dynode chains. It is powered with a transistorized base with a dynode (energy) and an anode (timing) outputs[24]. Fig.2.1 shows the detector assembly.

This detector was optimized for timing experiments and had a good pulse shape

TABLE 2.1

Some Properties of the NE213 Scintillators

Density (g/cm^3)	0.874
Refractive Index	1.508
Boiling Point, ^{o}C	141
Light Output,(% Anthracene)	78%
Decay Constant, Main Comp. (ns)	3.7
Wavelength of Max. Emission (nm)	425
No. of H Atoms/ No. of C Atoms	1.213
Principal Application	fast n(PSD)

Fig. 2.1 . The two main parts of the NE213 scintillator : the 10" scintillation cell and the 5" photomultiplier.

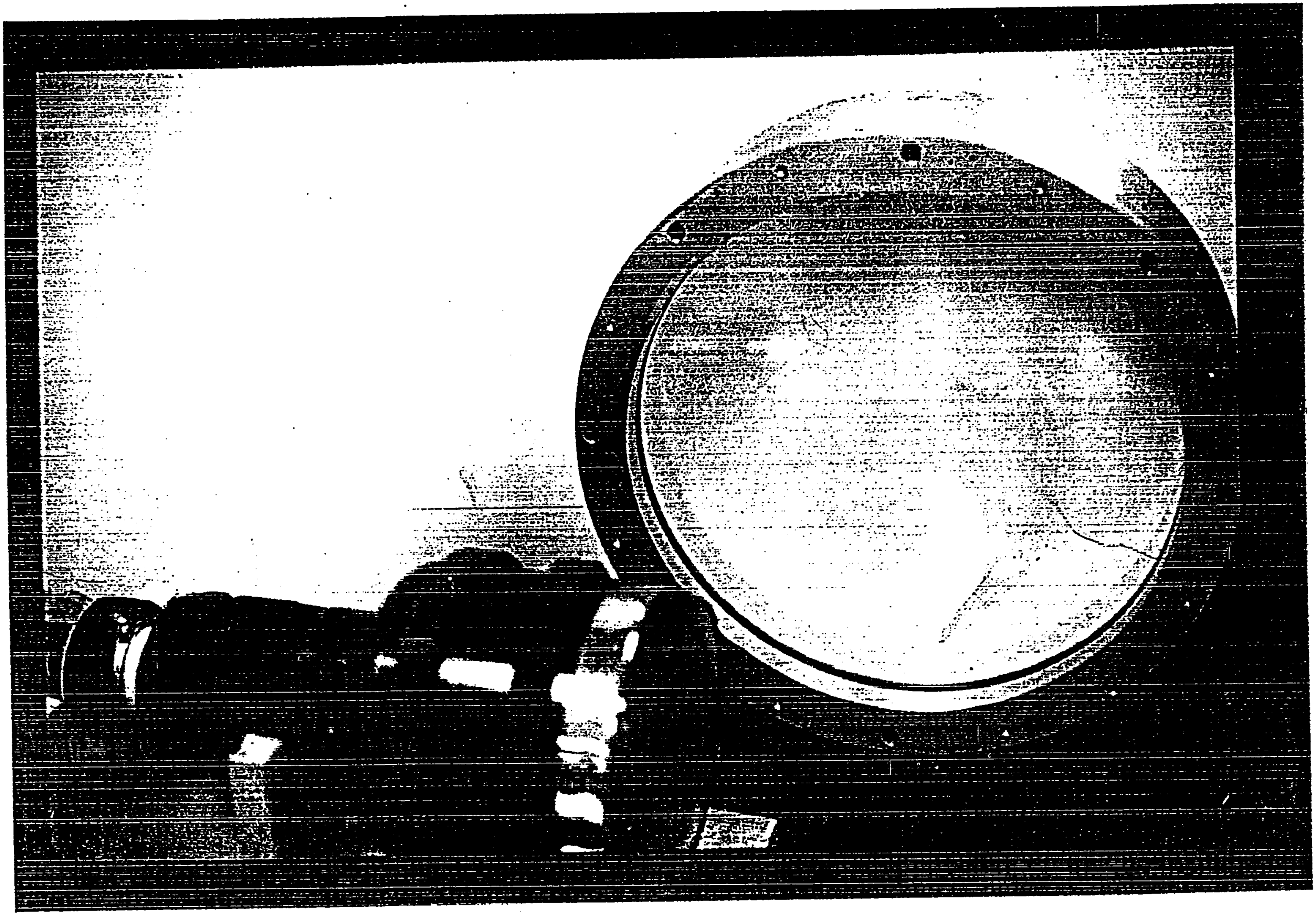

Discrimination (PSD) properties. The energy resolution of the detector, however, was poor. The reason behind this is that the direct coupling of a small PM tube with a large scintillator produces a non-uniform light signal collected at the photocathode of the PM tube. The light signals generated at the center of the scintillator are directly detected by the PM tube while light signals generated near the edges of the scintillator encounter multiple reflections with the boundaries of the Al-reflector of the scintillator cell before reaching the PM tube. When they reach the PM tube , their amplitudes have decreased because of scatterings. As a result of non-uniform light output, a particle produces less light when it hits the edge of the scintillator as compared to the case when it hits the detector center. For an energy bias set corresponding to light output of particle incident at the center, the particles incident on the edges are not counted. This results in decreased efficiency of the detector. A way to resolve this problem is to use a PM tube having the same diameter as the large scintillator. PM tubes with small diameter, however, are preferred because of their high quantum efficiency. Therefore, the best solution is to incorporate a conical light guide with diameters matching the scintillator and the PM tube. The non-uniformity in light collection is removed by incorporating a light guide (LG) as shown in fig.2.2.

In the present work, a conical plexi-glas light guide of 100 mm height, 250 mm base diameter and 130 mm top diameter was used to couple the 5"(130 mm) photomultiplier tube with the 10" (250 mm) diameter NE213 cell. The light guide was partially painted with NE560 reflector paint using the scheme mentioned by Scholermann et.al.[25]. Since the top and bottom of the light guide provide the optical coupling, they were not painted. The sides of the light guide were painted

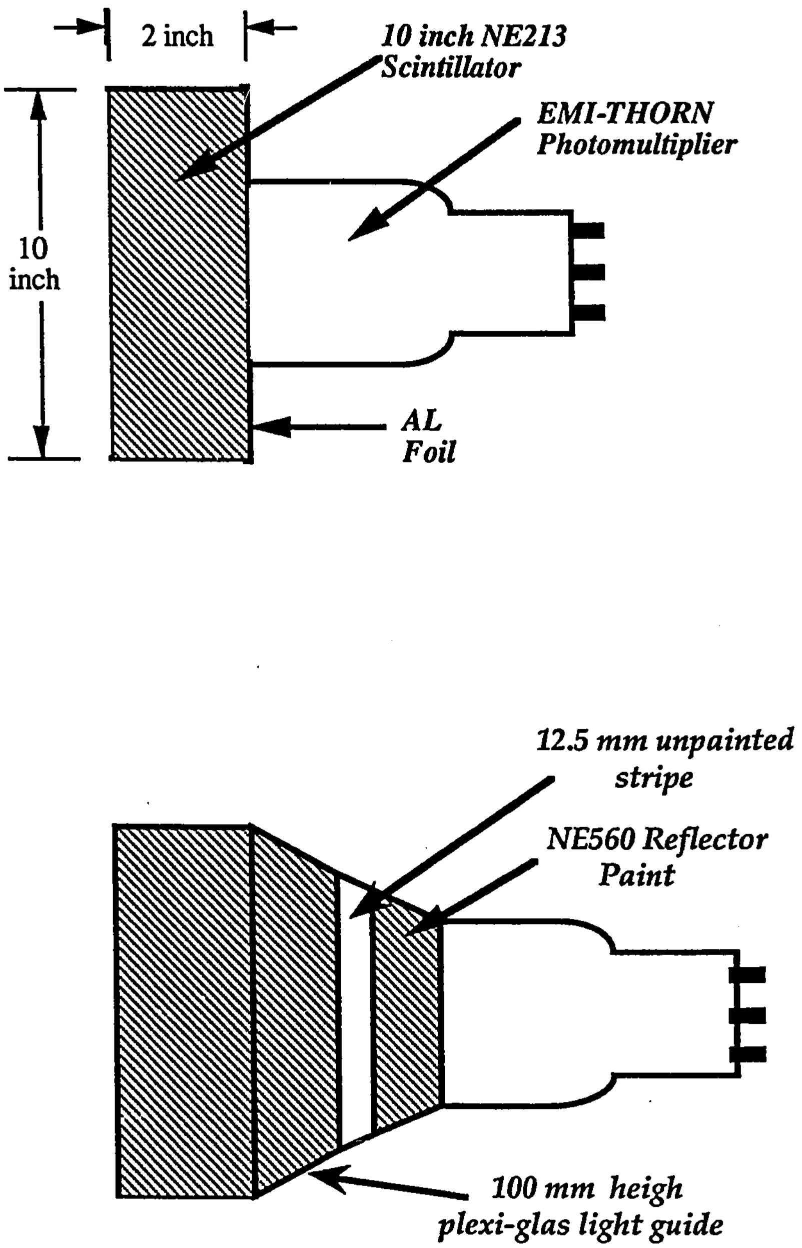

Fig.2.2. A schematic diagram of the 10" scintillator before and after incorporating the light guide.

leaving a stripe of width of 12.5 mm unpainted at a height of 45.8 mm from the base of the light guide. According to Scholermann[25], painting the light guide with this proportion will result in a uniform light signal. In order to incorporate the light guide, the original detector was deassembled into its two components: the scintillator cell and the PM tube. The optical grease NE586 was applied on the top and bottom of the light guide (the refractive index of NE586 is close to that of glass). Then the 250mm side of the light guide was placed on the scintillator cell glass window. The reflectivity was then increased by covering the light guide with aluminium foils. After that, a housing was built around the lightguide. It consists of Al-rings and rubber light-tight seals stacked together using long threaded screws. Finally, the PM tube was mounted on the lightguide. The original outer case assembly of the PM tube was bolted with aluminium housing of the light guide. In order to make the detector assembly fully light tight, a plastic tape was wrapped around the detector assembly. Fig.2.3 through 2.7 show the different stages followed in the assembly of the detector with the light guide.

Fig.2.3. The original 10" scintillator in direct coupling to the 5" photomultiplier.

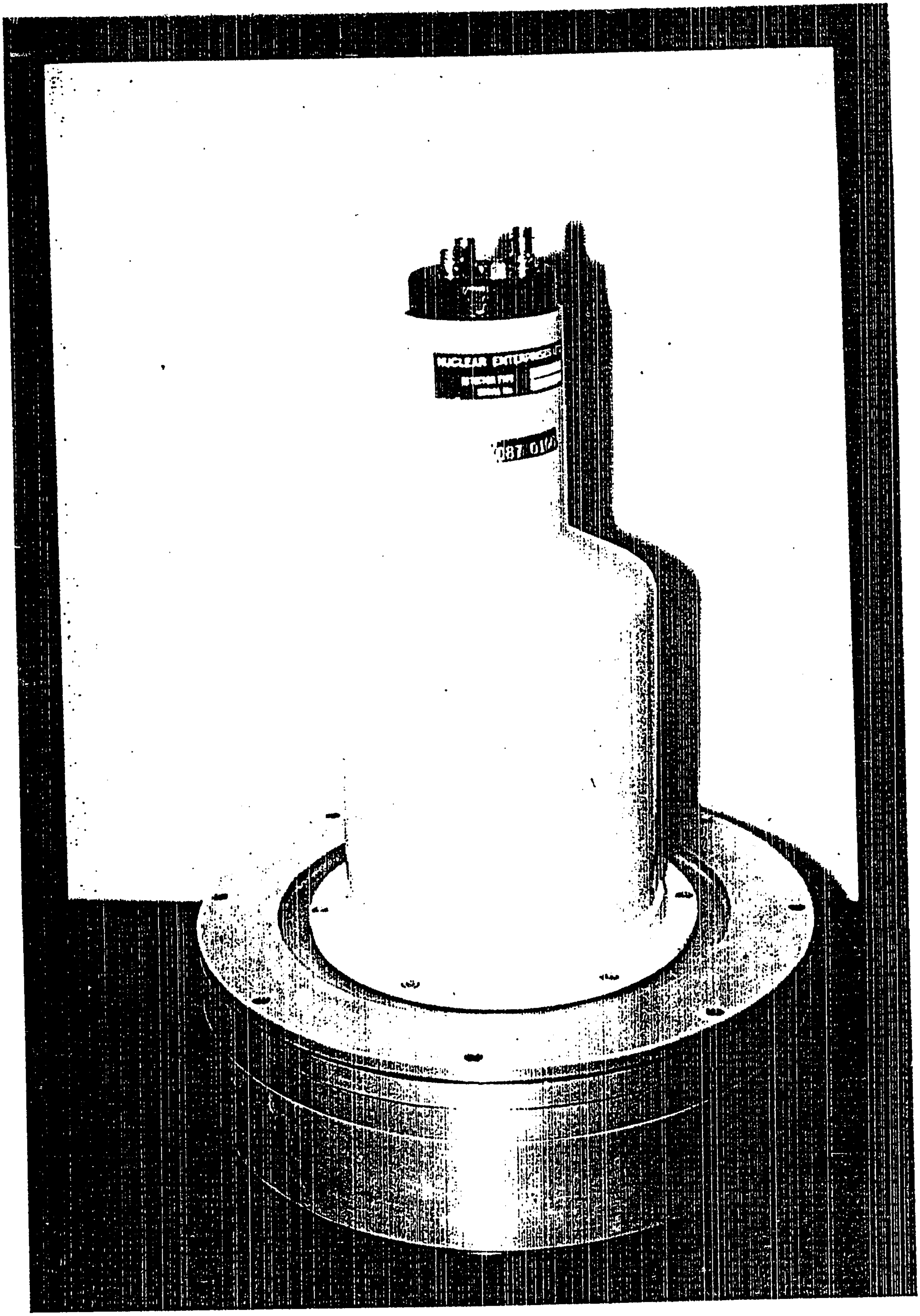
NUCLEAR ENTERPRISES
087 01

Fig.2.4. The Upper Cover That Holds the 5" Photomultiplier to the 10" Scintillator Is Removed.

3

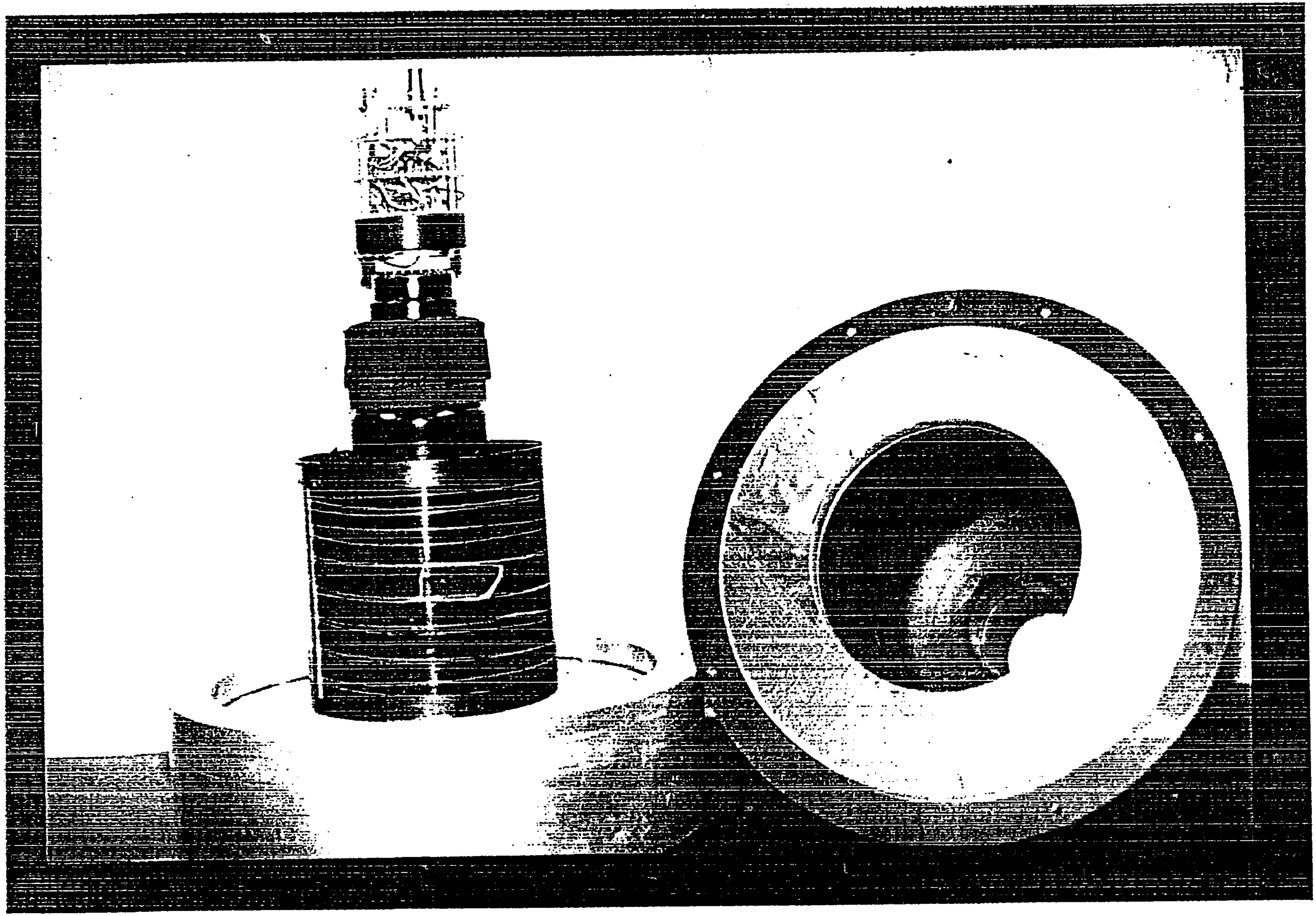

Fig.2.5. The 10" Base of the Painted Conical LG Is Optically Coupled to the 10" Scintillator by the Optical Grease NE586.

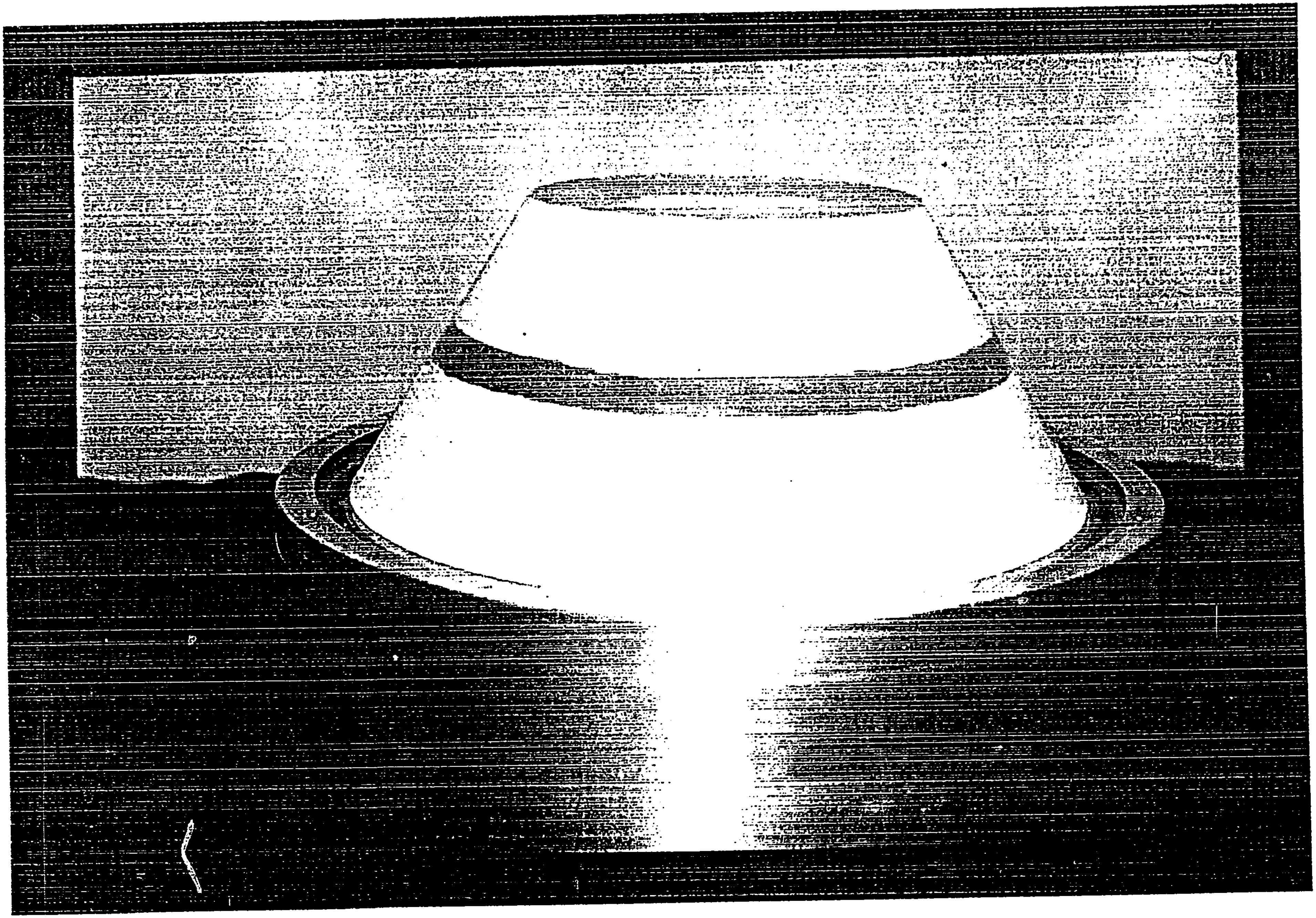

Fig.2.6. The 5" Base of the LG is Optically Coupled to the 5" Photomultiplier. To Enhance the Reflectivity, the LG Is Covered with Aluminum Foils.

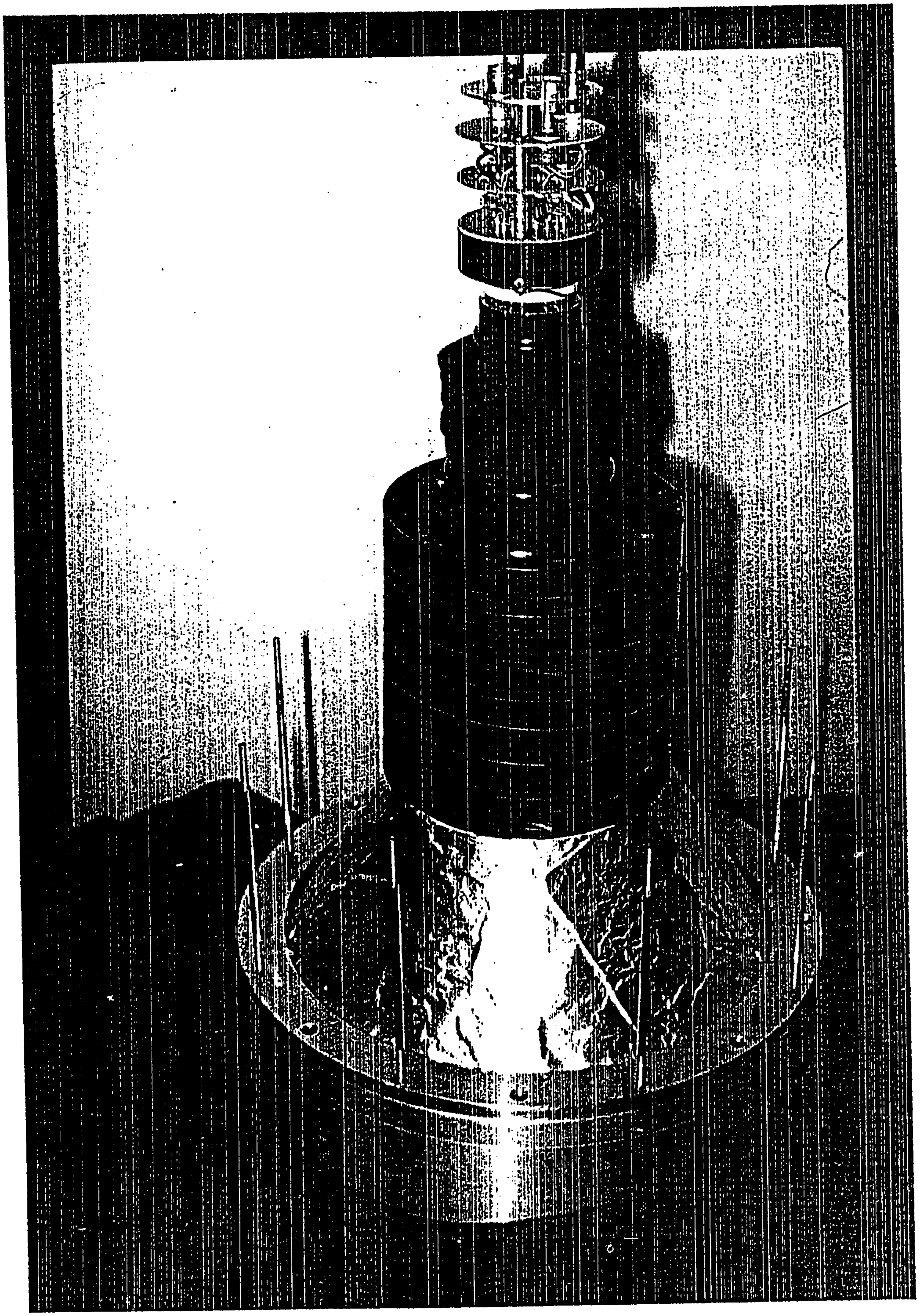

Fig.2.7. The Modified Detector in It's Final Shape; the 10" Scintillator is Coupled to the 5" Photomultiplier Through the LG.

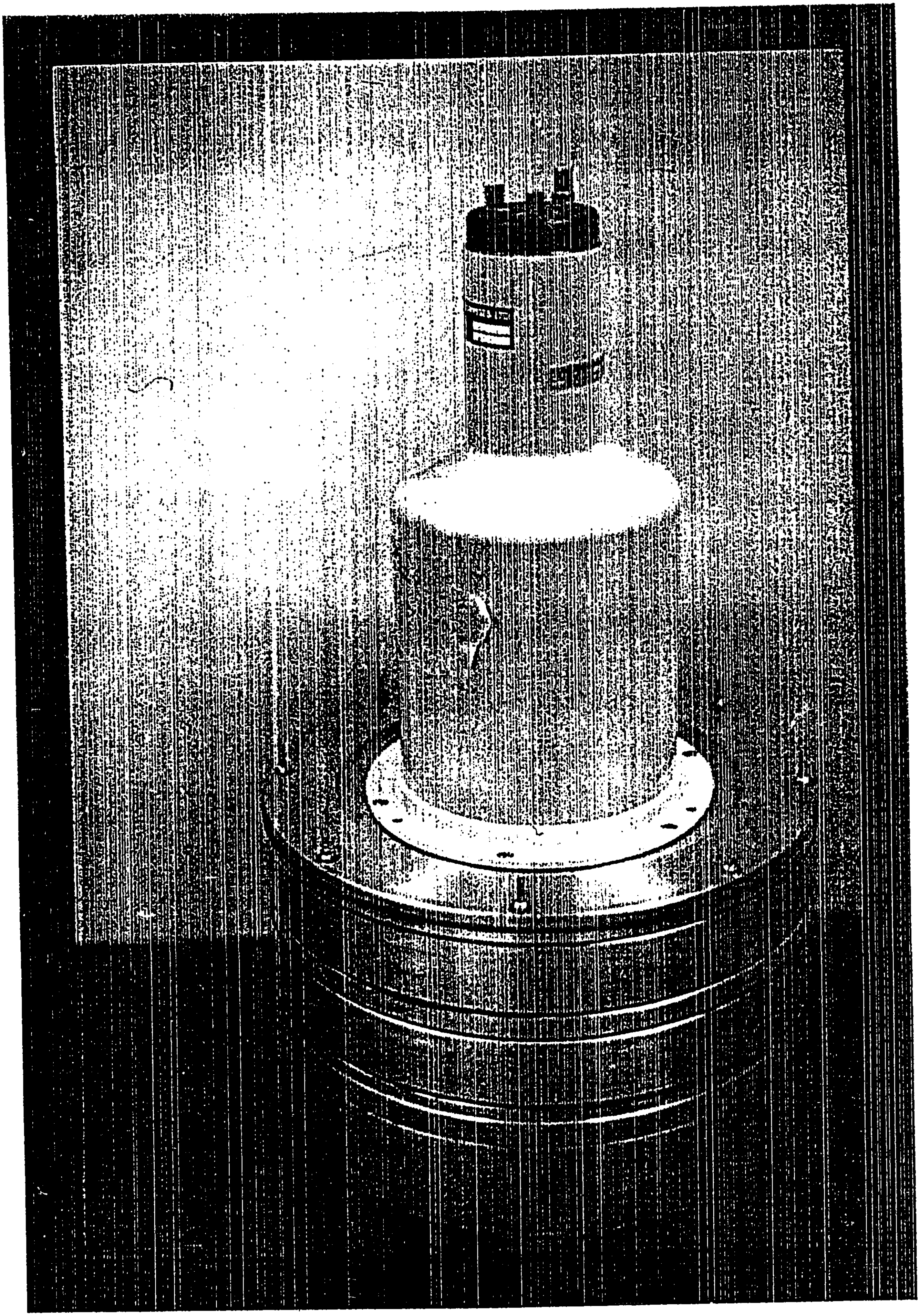

CHAPTER THREE

PERFORMANCE TESTS

The effect of incorporating a light guide (LG) between a scintillator and a photomultiplier having a smaller diameter, on the properties of this detector should be studied before making any further experimentation with this detector. Out of the several good properties the NE213 scintillator has, energy resolution, time resolution, and pulse shape discrimination are the most important in efficiency measurements, the goal of this project. For this reason, this chapter is devoted for testing the performance of the detector.

Performance tests of the 10"(250 mm) scintillation detector were carried out using standard gamma ray sources and Am-Be neutron source. In these tests, the detector energy resolution, time resolution and pulse shape discrimination properties were investigated. In order to study the effect of the light guide on the performance characteristics of the detector, the tests were performed for the detector with and without the light guide.

3.1. ENERGY RESOLUTION TEST

When a monoenergetic gamma ray is incident on an organic scintillator it interacts with the free electrons through the Compton interaction. The resulting Compton electron distribution is dependent on the angle of scattering and is represented by a Compton edge. Theoretical calculations show that the intensity of the Compton electrons is maximum at 180 degrees and fall sharply to zero at this angle. The energy of Compton electrons at this angle is maximum, and hence the energy can be determined from knowing the position of the cut. In real experiments, however, because of limited resolution of the detector used, the edge is diffused and the exact energy of the Compton electrons having maximum energy can not be exactly defined. Therefore it was a standard practice to take the half-height of the edge L_h as the position of Compton electrons having maximum energy[1]. Later it was found out that the maximum energy of the electrons is somewhere between the position of maximum counts and that of the half-height[26]. For this reason a new technique, in which only electrons encountering head-on-collision, are recorded, was introduced. In this technique, called the Gamma-Gamma Coincidence technique[26], the 180 degrees backscattered gamma rays are recorded by a reference detector. If the energy of the backscattered gamma rays, results in a head-on-collision, then the event is recorded. All events corresponding to other scattering angles, are therefore suppressed. The resulting spectrum is a gaussian peak whose centroid represents the Compton electron energy and the FWHM divided by the centroid gives the energy resolution. The width of the peak depends on the resolution of the detector.

Dietze et al.[21]have thoroughly investigated the pulse height response of the NE213 detector for various gamma ray energies. They have compared the measured energy resolution with the calculated one using a Monte Carlo code. They also calculated the deviation of conventional calibration L_h from the true maximum energy of Compton electrons E_c which was measured in Gamma-Gamma Coincidence experiment. The interesting results of their study was the dependence of the deviation of parameters, and hence, the energy resolution on the energy of gamma rays and on the detector size.

3.1.1. Experimental Procedure

The energy resolution test of the 10″ scintillator were carried out using the Gamma-Gamma Coincidence technique[26]. In this test, a 5″x5″ cylindrical NE213 liquid scintillator was used to record the backscattered gamma rays. One of the gamma sources listed in table 3.1 was attached to the aluminium housing at the center of the 10" scintillator, which is about 2 mm thick. The energy signals from both detectors were fed into preamplifiers. The signals were then transmitted by long cables to signal processing electronics and were further shaped and amplified by Double Delay Linear Amplifiers (DDL). In order to generate coincidence gate, the DDL output of the amplifiers were fed to Timing Single Channel Analyzer (TSCA) units. The energy windows of both TSCAs were set by proper adjustment of the Lower Discriminating Level (LLD) and the Upper Discriminating Level (ULD) of the TSCA modules. The energy window for the detector understudy was maximum i.e., zero LLD and maximum ULD,while a small energy window corresponding to the energy of the Compton electrons induced by backscattered gamma rays was set for the monitor detector. As shown in table 3.2, the maximum energy of Compton electrons due to backscattered gamma rays does not vary much with incident gamma ray energy, therefore the TSCA window remains fixed. By adjusting the delays in each TSCA, their output signals were brought into time coincidence. These two signals were then fed into a Universal Coincidence (UC) unit whose output was used to generate a gate through a Gate and Delay Generator (GDG) module. The gate and the DL output of the detector undestudy amplifier were fed to the data acquisition system. There the DL signal was fed to the linear input of a CAMAC ADC, while the GDG output was connected to the gate input of the CAMAC ADC which is an integral part of the ERL data acquisition system based around VAX 11/785. The details of the ERL data acquisition system will be given in section 3.1.2. Fig.3.1 shows the electronics used in this experiment .In gated mode of ADC coincidence peak was acquired while the Compton edge of the same source was acquired in the ungated mode of the ADC. These measurements were repeated for ^{137}Cs, ^{54}Mn , ^{65}Zn and ^{22}Na gamma sources. The data was acquired with the detector before and after incorporating the light guide. In order to show the effect of the light guide on the energy resolution of the detector, energy resolution results will be presented for the detector with and without light guide.

TABLE 3.1

Data of Gamma Sources Used in the Energy Resolution Test and for Calibration

Gamma Source	Gamma Ray Energy (MeV)	Half-Life
^{22}Na	0.511	950.4 d
^{137}Cs	0.662	30 yr
^{54}Mn	0.835	312.5 d
^{65}Zn	1.115	244 d
^{22}Na	1.275	950.4 d

3.1.2 Data Acquisition and Analysis System

Physical events derived from detectors used in the tests mentioned in this chapter are acquired and processed using a data acquisition and analysis system at the Energy Research Laboratory (ERL). This system is built around a 2-node, single-CPU, VAX 11/785 cluster. In this system, experimental data is acquired using number of LeCroy 3511 fast CAMAC Analog-to-Digital Converter (ADC) modules. They accept linear signals in the anticoincidence mode and linear and gate signals in the coincidence mode. The ADCs digitize the experimental data and send them to a Microprogrammable Branch Drive (MBD), a 16-bit microcomputer, which operates as an interface between the CAMAC and the VAX computer. The spectra these data generate are displayed on Tektonix graphics terminals.

The data acquisition system uses XSYS software package developed for the VAX computer. The data acquisition program consists of three files namely COM, DAP and EVL files. A COM file contains XSYS commands which are excuted at various stages of the experiment. The DAP file (Data Acquisition Program) is a CAMAC and subprocess control file. It contains CNAF commands for CAMAC crate configuration and information on the VAX data buffer size. The EVL (Event Analysis Language) file contains the sorting algorithms for the individual ADC and its MBD channel. The data acquisition code used in the tests mentioned in this chapter is given in appendix A. Detailed information regarding the ERL data acquisition software and hardware may be found in references 27 and 28.

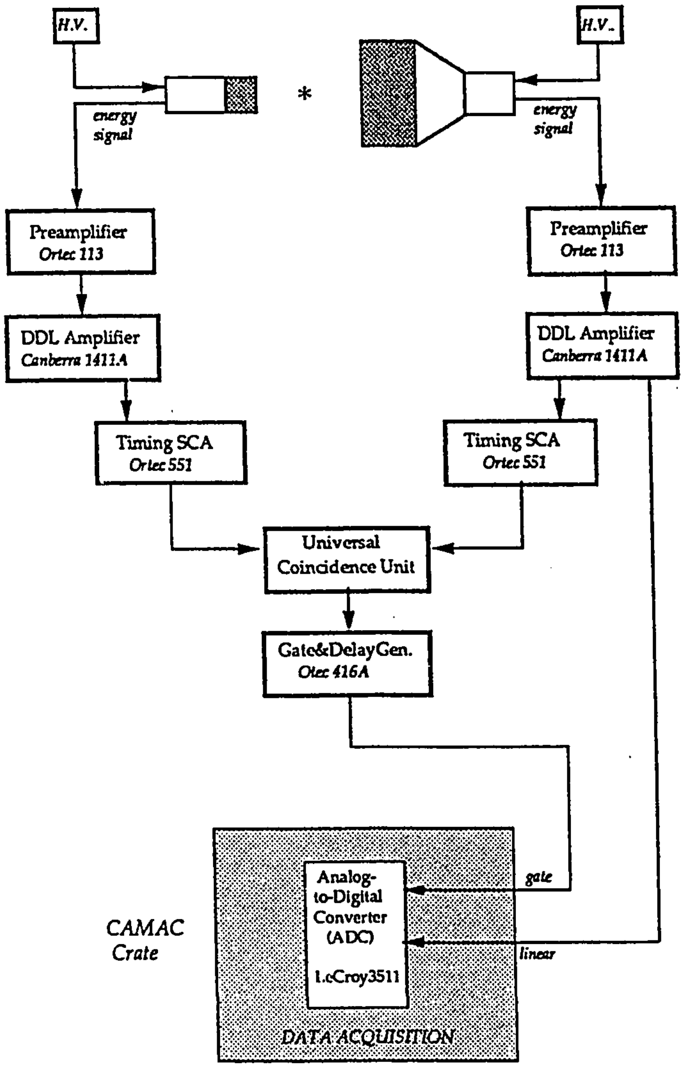

Fig.3.1. Schematic diagram of the electronics used in the energy resolution measurements.

TABLE 3.2

The Maximum Energy of Compton Electrons Detected by Each Detector (MeV)

Incident Gamma Ray Energy	Max. Energy of Compton Electrons due to Incident Gamma Rays	Energy of Gamma Rays Backscattered by Compton Electrons	Max. Energy of Compton Electrons due to Back-scattered Gamma Rays
0.511	0.341	0.170	0.068
0.662	0.477	0.185	0.078
0.835	0.639	0.196	0.085
1.115	0.907	0.208	0.093
1.275	1.061	0.214	0.098

3.1.3. Results and Analysis

Due to non uniform light collection, the energy resolution of the detector without the LG was very poor and the Compton edges and the coincidence peaks obtained with the 10" scintillator without lightguide contained no valuable information on the energy resolution of the detector. The determination of L_h from the Compton edge for calibration purposes was not possible since the uncertainty in locating the position where the counts are maximum was very large. As shown in Fig.3.2, the Compton edge taken with the ^{137}Cs source is not sharp enough to determine L_m. This indicates a poor energy resolution of the detector which is clearly shown by the corresponding Gamma-Gamma coincidence peak superimposed on Compton edge in Fig.3.2. Apart from this the peak has non gaussian distribution. A gaussian shape is needed in order to determine the centroid which correspond to Compton electrons with maximum energy and the FWHM which is related to the energy resolution of the system. An attempt was done to find the energy resolution with this configuration by assuming a gaussian shape having a centroid and a FWHM and taking very large error into account. The energy resolution of the detector was obtained only for ^{54}Mn and ^{137}Cs sources for which noticeable peaks were observed. The data is shown in table 3.3.

For the configuration with the lightguide in, the detector spectra were totally different. Fig.3.3 shows the Compton edge and the Gamma-Gamma coincidence peak of ^{137}Cs taken for the detector with the LG.The edge is sharp

TABLE 3.3

Comparison of energy resolution data before and after incorporating the light guide LG.

Electron Energy (MeV)	ΔEc/Ec (%) without LG	ΔEc/Ec (%) with LG
0.477	59	33.4
0.639	61	28.5

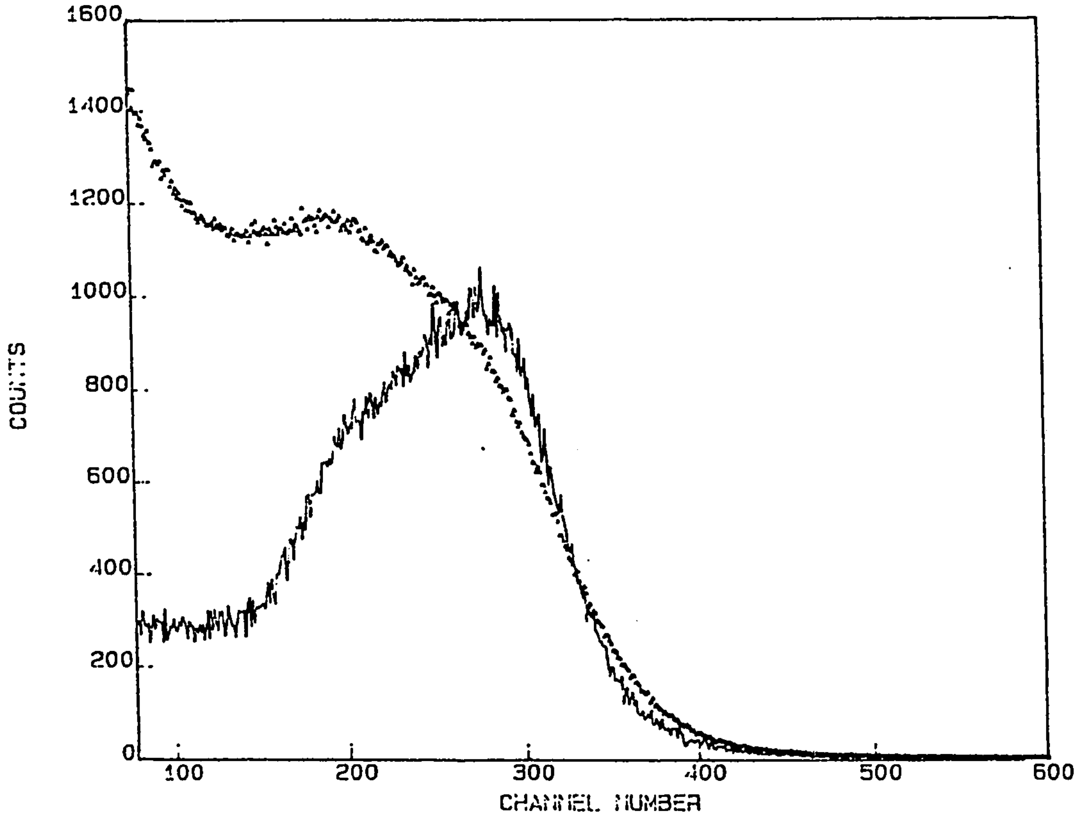

Fig.3.2. The Compton edge and the coincidence peak taken with the ^{137}Cs gamma source before incorporating the LG.

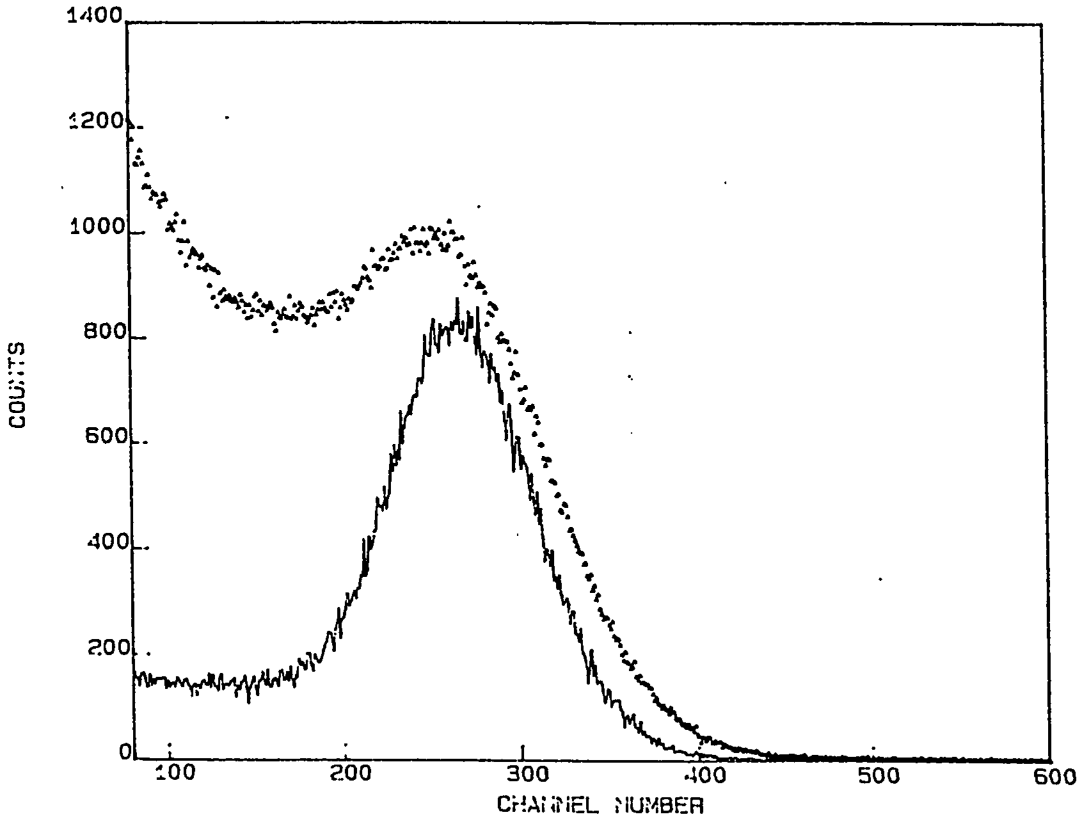

Fig.3.3. The Compton edge along with the coincidence peak taken with a ^{137}Cs gamma source after incorporating the LG

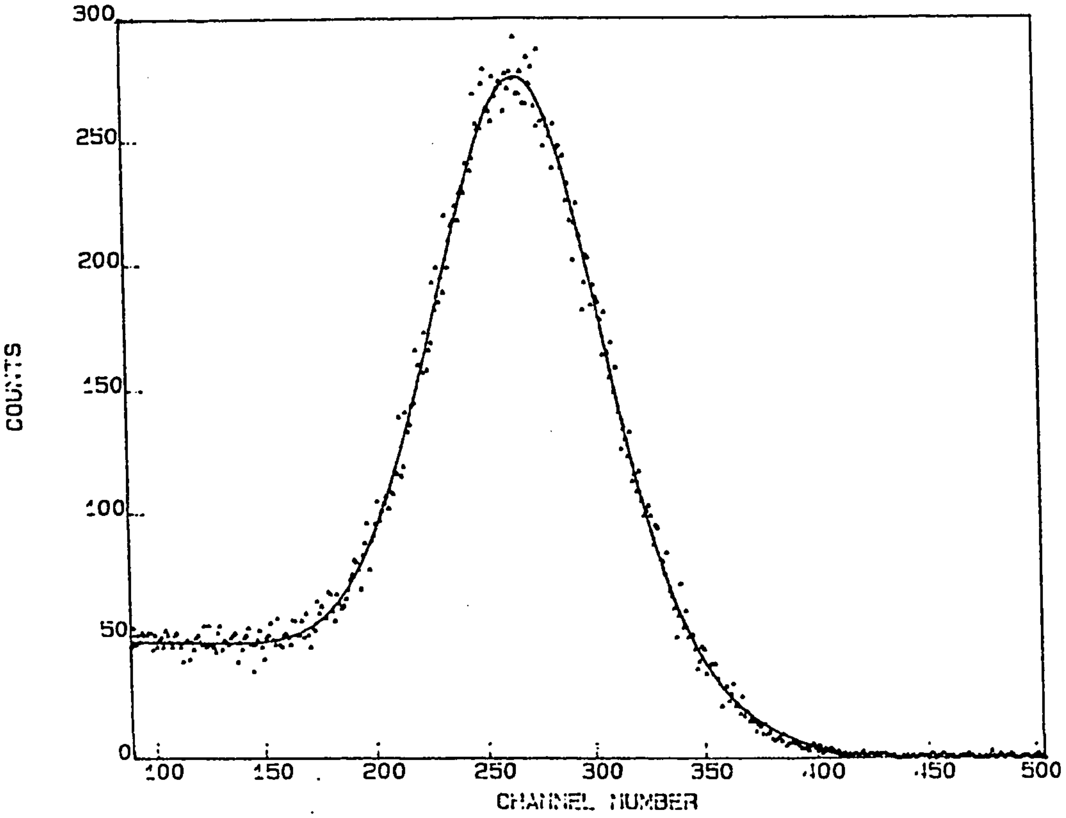

Fig.3.4.The gamma-gamma coincidence peak taken with the ^{137}Cs Gamma Source along with a polynomial fit.

and peak is gaussian. One could easily fit a gaussian peak with a polynomial background to get its centroid position and FWHM. Fig.3.4 shows a Gamma-Gamma coincidence peak fitted with a Gaussian peak superimposed on a polynomial background. From the centroid of the peaks for different Gamma rays sources, the energy calibration scheme of the detector was derived which was later used to convert FWHM into energy ΔE_c .Then the energy resolution $\Delta E_c/E_c$ was calculated using the true electron energy E_c. For the sake of comparison table 3.3 shows the energy resolution data for the detector with and without the lightguide. An improvement of about 50% was achieved in energy resolution at 0.639 and 0.477 MeV energies after incorporating the LG.

Table 3.4 shows the energy resolution data of the detector with LG along with the values reported by Dietze [21] . The good agreement between our values and Dietze values reflects the good coupling achieved in our detector. The table also shows the deviation parameter $(E_h-E_c)/E_c$, which is a measure of the deviation of the conventional energy calibration point E_h from the true energy E_c. The energy resolution $\Delta E_c/E_c$ of our 10" scintillator varies from 33.4 to 18.0% over the electron energy range of 0.3 to 1.1 MeV. Although the deviation is large but the trend is that as the electron energy increase, E_h moves towards E_c. It improves from 21.2 % at 0.3 MeV to 15.4 % at 1.1 MeV. The large error in the deviation parameter for the ^{65}Zn source due to weak source which has a half-life of 244 days. It was being used since 1988 and its activity was reduced from 1.022 mCi at that date to about 0.3 mCi at the date of performing the experiment. Also, due to the high energy of the gamma ray (1.115 MeV) for ^{65}Zn, the Compton scattering compete with the pair production, hence reducing the events of

TABLE 3.4

Energy resolution data of the modified 10"diameter NE213 scintillator compared with Dietze[21] data for different gamma ray energies.

Electron Energy (MeV)	$\Delta E_c/E_c$ (%)		$(E_h-E_c)/E_c$ (%)	
	Present Work	Dietze Data	Present Work	Dietze Data
0.341	33.4	32.5	23.8	14.7
0.477	28.0	30.0	20.3	13.0
0.639	23.7	24.0	17.5	-----
0.907	18.3	20.0	17.6	-----
1.061	18.0	17.0	15.5	-----

Compton scattering. The energy resolution data of the present work are in good agreement with those of Dietze. The values of the parameters $(E_h-E_C)/E_C$, obtained in this experiment are larger than those obtained by Dietze which indicates better coupling of their detector.

An empirical fit was made to the energy resolution data of the 10" scintillator as a function of the electron energy using the relation[29]

$$\Delta E_c/E_c = \left[\alpha^2 + \beta^2/E_c + \gamma^2/E_c^2\right]$$

Table 3.4 show the values of the resolution parameters α , β , and γ along with the values of Dietze. The parameter β mainly determines the energy resolution. The value of β obtained from our fit is 3% higher than that of Dietze. As β is related to the statistical behavior of the light production processes depending on photomultiplier , detector photomultiplier coupling etc ., one expects a difference between our values and Dietze values. Fig.3.5 shows the energy resolution $\Delta E_C/E_C$ plotted as a function of the compton electron energy E_C along with the empirical fit.

TABLE 3.5

Comparison of the detector resolution parameters found in the present study for the 10" detector and those reported by Dietze et al.

Parameter (%)	Present Work	Dietze et al.
α	5.6	5.6
β	18.5	18.0
γ	0.2	0.2

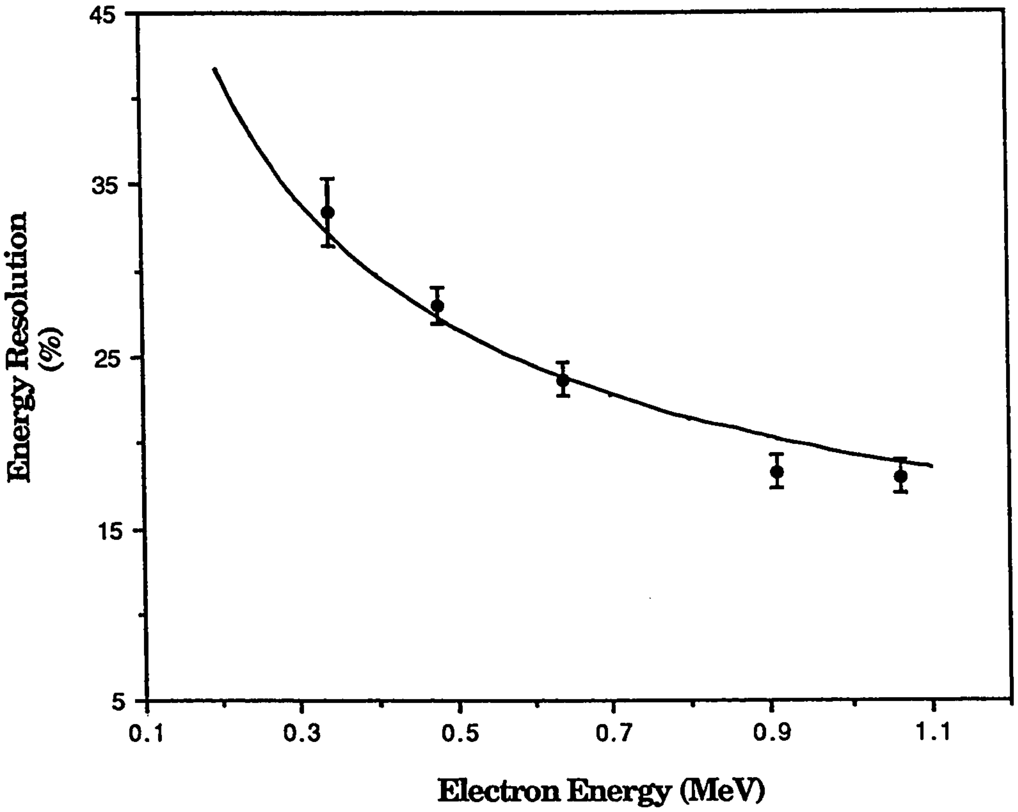

Fig.3. 5. Pulse height dependent resolution $\Delta E_C/E_C$ for the 10" NE213 liquid scintillator.

3.2. TIME RESOLUTION TEST

The contribution to time resolution of scintillation detectors are associated with three phases of the timing process: time variations in the interaction of radiation with detectors, time variations arising in the formation of the detector signal- these originate both in the scintillator and the photomultiplier tube, and time variations associated with the time derivations devices. Time spreads in photomultipliers mainly originate between the photocathode and the first dynode. It has been confirmed experimentally[30] that for cylindrical scintillators, the time spread of light collection on a photocathode can not be neglected when analyzing the results of timing experiments in the range of few hundreds of picoseconds.

The dependence of time resolution on energy is essentially contained in the average number of photoelectrons emitted from the photocathode. Due to the statistical nature of the process, the number of photoelectrons is distributed around the average number which is also reflected in the pulse height resolution.

The time resolution of the detector is usually measured with respect to a reference detector whose time resolution is known and it has a faster response than the detector under study. This reference detector and the detector under study are placed face-to-face and a source of gamma rays is put in between. This source should give time correlated gamma rays. Timing coincidence peak is obtained using a Time-to-Amplitude Converter (TAC) unit which is triggered by the reference detector. The FWHM of the resulting peak contains information on the time resolution of the two detectors in quadrature. Subtracting the contribution of the reference detector, the time resolution of the detector under study can be obtained.

3.2.1. *Experimental Procedure*

The time resolution of the 10" scintillation detector was measured with reference to a fast 5"x5" scintillation detector using a Time Coincidence technique [31]. In this test, a ^{60}Co gamma ray source which emit time correlated gamma rays of energy 1.117 and 1.33 MeV, was used. A schematic diagram of the energy levels of the ^{60}Co source is shown in fig.3.6. One of the gamma rays is detected in the reference detector while the other is detected in the detector under study. As soon as the event is detected in the detector a fast signal is produced by each detector.

At first, the dependence of the 10" detector time resolution on the energy bias was studied. The ^{60}Co source was attached at the center of the scintillator. Another 5"x5" NE213 fast liquid scintillator, located 80 mm from the other detector, was used as a reference detector. As in the energy resolution test, the shaped and amplified energy signals of the two scintillators were fed into Timing Single Channel Analyzers (TSCA) where they were brought into time coincidence. The

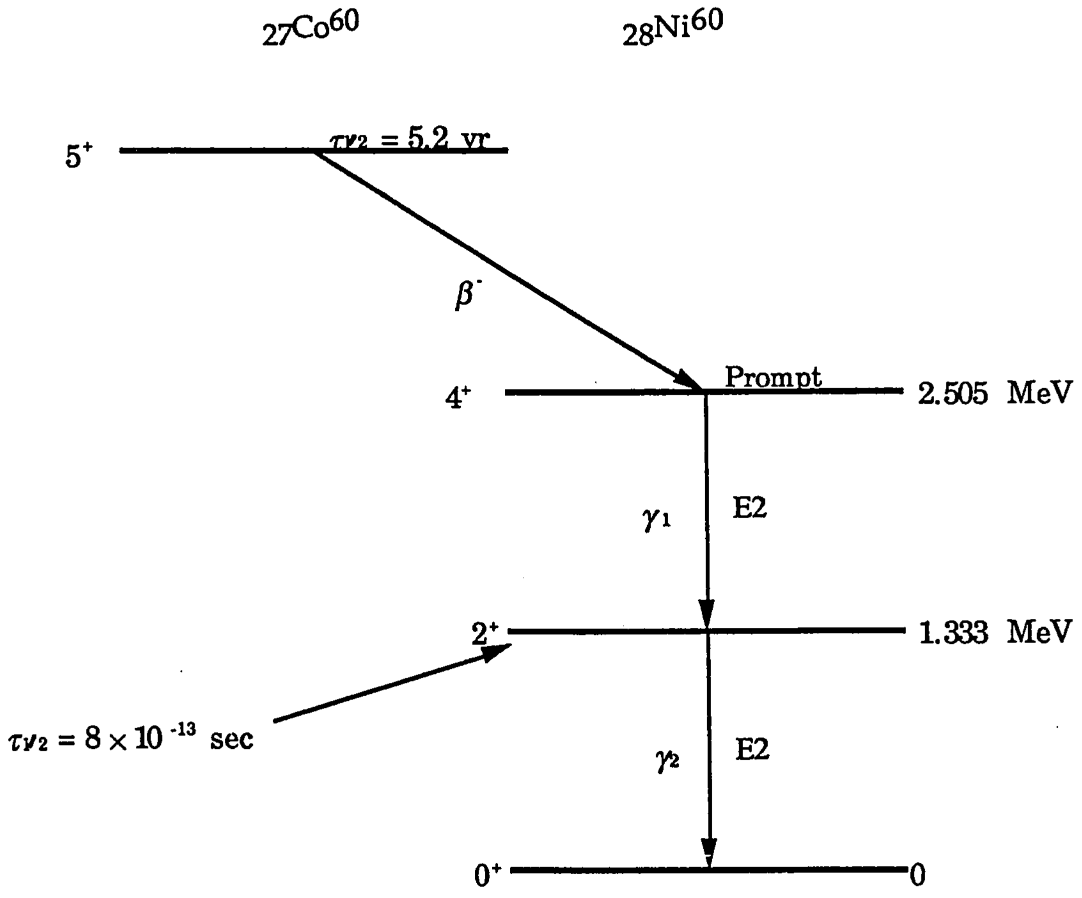

Fig.3.6. The decay scheme of the ^{60}Co time correlated gamma source

resulting signals were then fed into a Coincidence Unit and a gate signal was then The TAC is a unit that accepts two signals, a *start* and a *stop* signals, and generate produced through a Gate and Delay Generator (GDG) unit. Time signals from the two detectors, on the other hand, were fed into two Constant Fraction Discriminator (CFD) modules which generate fast triggering signals showing the time of occurrence of the event. The time signal of the 5″ detector was sent then to a Time-to-Amplitude Converter (TAC) module as a *start* signal. The *stop* signal was the delayed 10" scintillator time signal. The TAC gives an output signal whose amplitude is proportional to the time difference between the two signals. The output of the TAC along with the GDG gate signal were sent to the date acquisition system mentioned previously.

In order to study the dependence of the time resolution of the system on the energy bias, the two discriminating levels of the TSCA modules were calibrated in terms of energy using ^{137}Cs and ^{22}Na gamma sources. The calibration was done using the channel corresponding to half height of the Compton edge which was taken as the maximum energy of Compton electrons. Four different energy windows with upper level corresponding to 0.25 , 0.34 , 0.48 and 0.64 MeV were selected. The width of each window was 10% of the upper energy. The GDG signal was used to gate the TAC signal for each of these four energies. The FWHM found for each of the obtained spectra represent the time resolution of the system at the given bias. In addition to this, the time resolution of the 10″ scintillator was measured at a lower level bias equivalent to energy of 0.5 MeV.

The FWHM of the peak obtained in this way represent the time resolution of both detectors ,i.e., the 10″ detector and the 5″ detector. In order to find the time resolution of the 10″ detector, the contribution of the 5″ detector to the time resolution should be subtracted in quadrature. The time resolution of the 5″ detector was measured separately using another 5″ detector. From measured FWHM of the obtained peak, the time resolution of the individual 5″ detector was calculated assuming that the contributions from the two 5″ detectors to be equal. Fig.3.7 shows the electronic set-up used in this test.

The output signal of the TAC needs to be calibrated in terms of time. This was achieved by using a precise Time Calibrator module. The start output of this module was connected to the start of the TAC and the stop to the stop. The Calibrator module generates successive stops after a preselected period. With the Calibrator, the TAC output consists of sharp equidistance spikes whose separation in channels corresponds to the preselected period of the Calibrator. Fig. 3.8 shows a typical time calibration spectrum. From the channel separation between two spikes and the known, preselected period, one can find time dispersion.

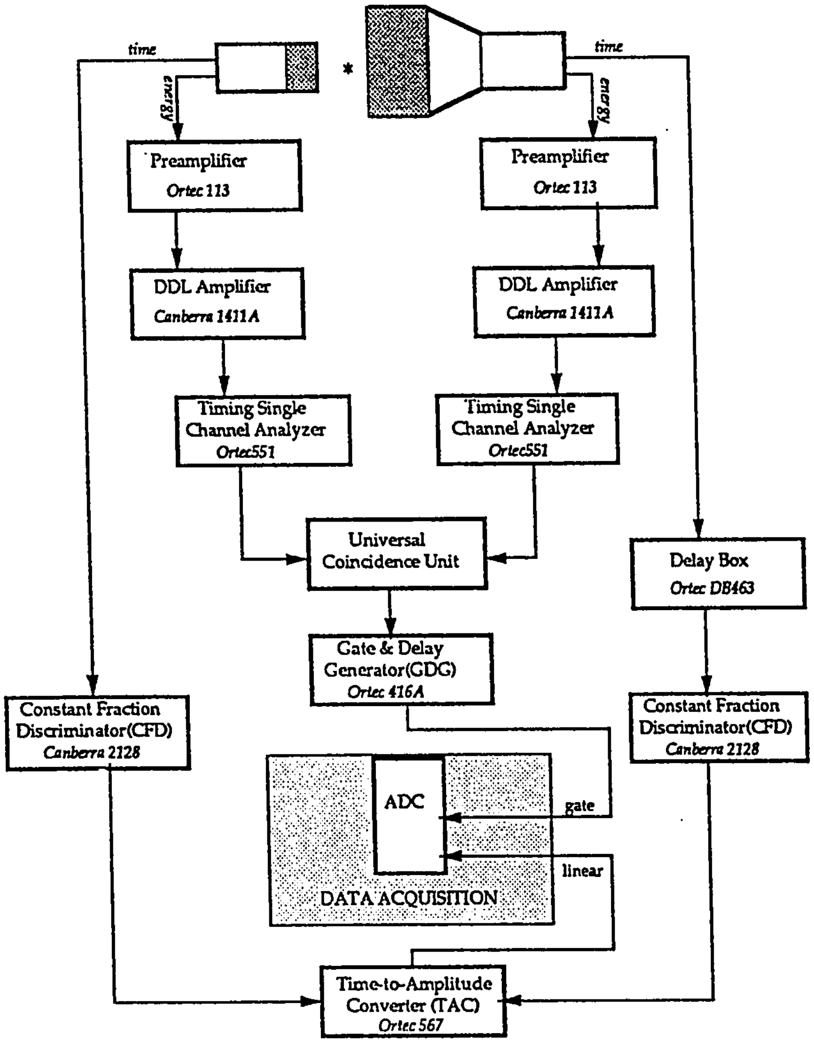

Fig.3.7. Schematic diagram of the electronics used in the time resolution measurements.

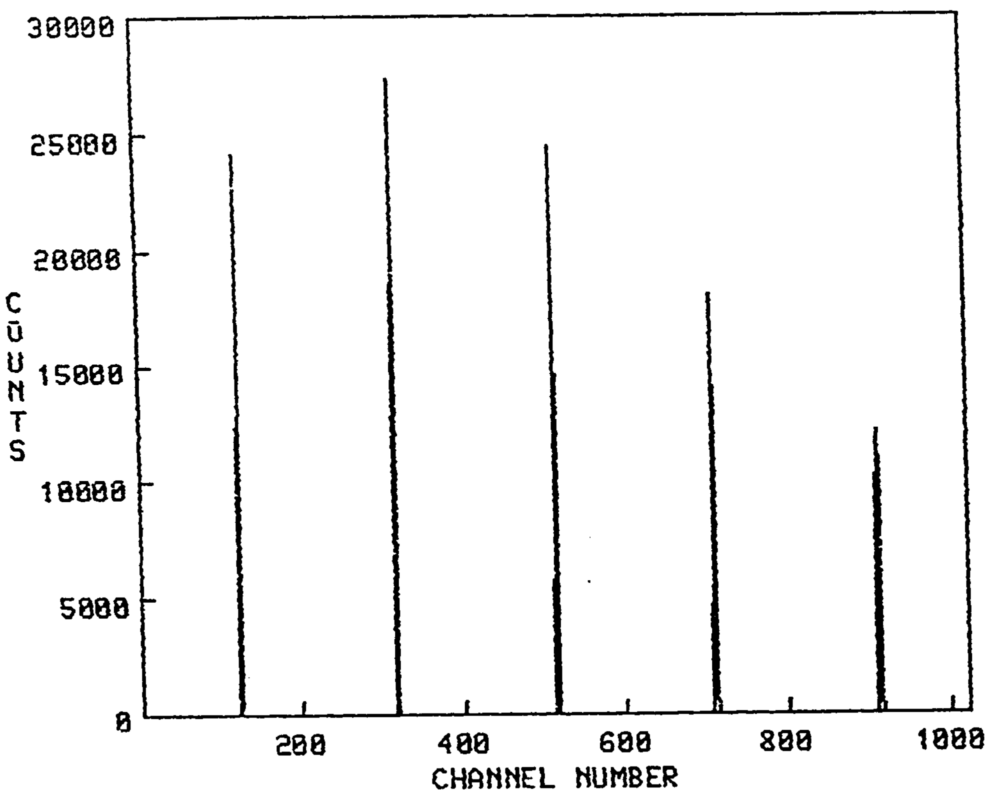

Fig.3.8. A typical time calibration spectrum generated using a Time Calibrator module.

3.2.2. Results and Analysis

The results of first study .i.e., the dependence of time resolution on the energy bias are shown in table 3.6. As can be seen, the time resolution deteriorates as the energy decreases. This is due to the fact that the events with higher energy bias have less noise contribution. Fig.3.9 shows the relation between time resolution (FWHM) and energy. The straight line relationship proves that time resolution depends on the inverse sequare root of the energy (FWHM vs. 1/ sqrt(E)).

The time resolution of the 10″ scintillator with and without the lightguide were measured separately at a bias of 0.5 MeV electron energy. The first measurement was for the system consisting of the 10" and the 5" scintillators. Fig.3.10 shows the peak obtained along with a gaussian fit .The resulting FWHM is the quadratic sum of the fwhm from the two detectors as given by

$$FWHM = \sqrt{(fwhm)^2_{10''} + (fwhm)^2_{5''}}$$

This shows clearly that in order to know the fwhm of the 10″ detector the fwhm of the 5″ detector must be known . For this reason we replaced the 10″ detector with a 5″ detector assuming it has the same time resolution as the original 5″ detector . In this case the above equation reduces to

TABLE 3.6

The dependence of time resolution on the energy bias

Bias (MeV)	FWHM (ns)
0.25	1.749
0.34	1.596
0.48	1.507
0.64	1.400

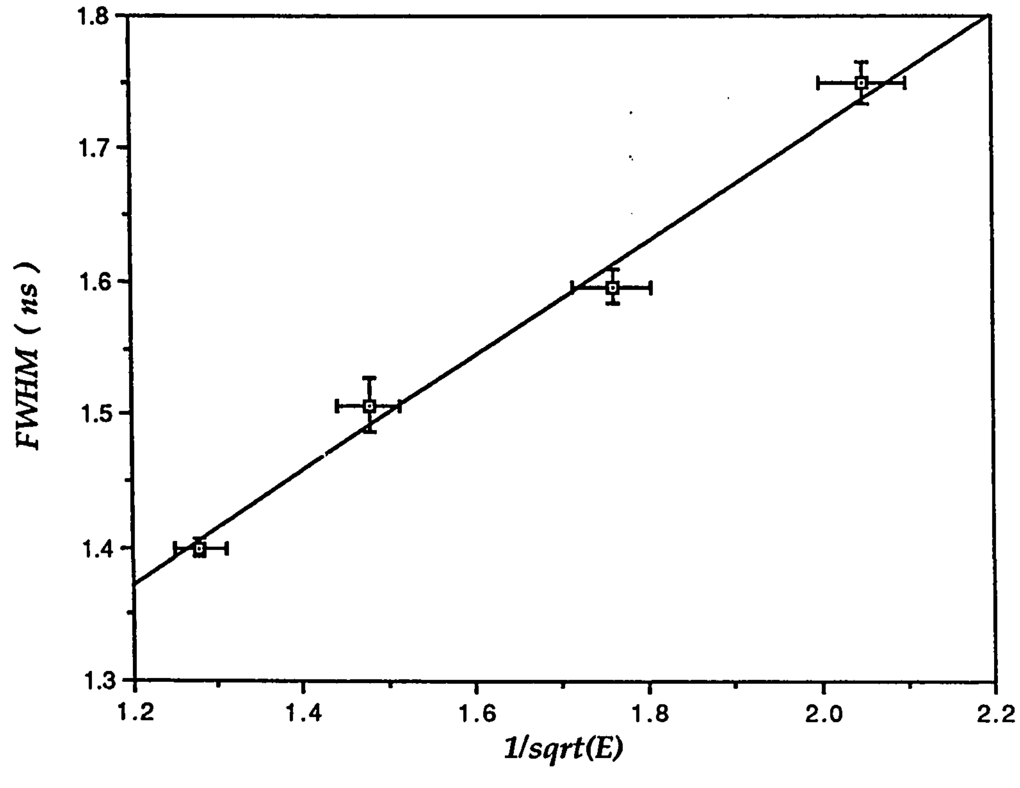

Fig.3.9. The dependence of time resolution on the energy bias

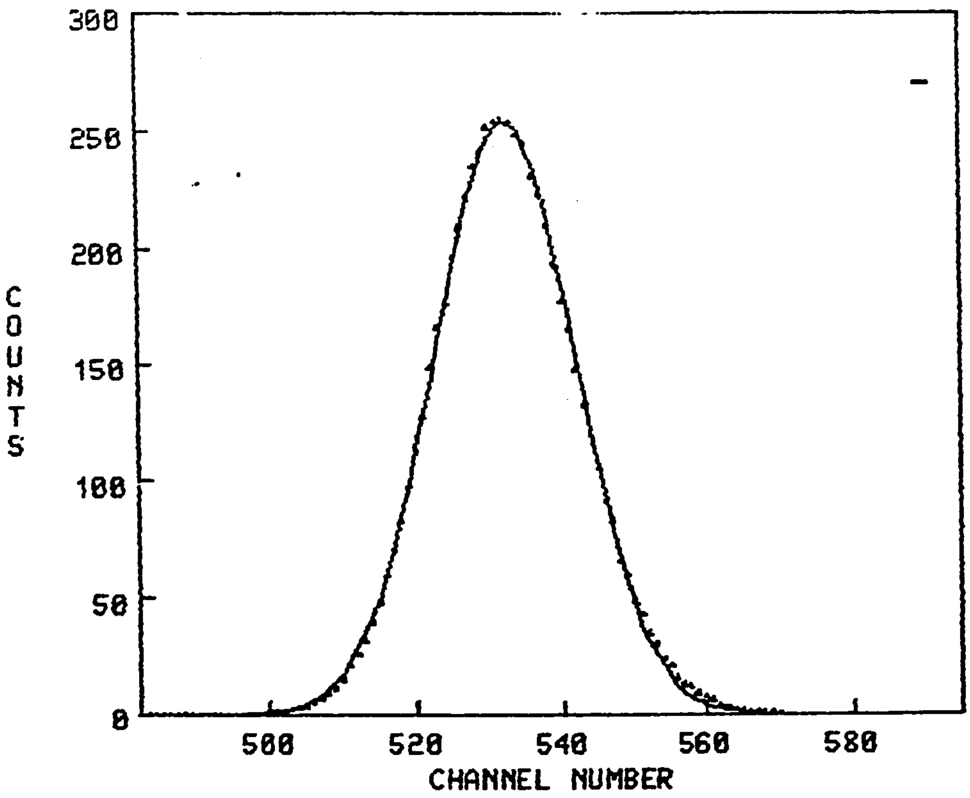

Fig.3.10. A typical time coincidence peak along with a gaussian fit.

$$FWHM = \sqrt{2}(fwhm)_{5''}$$

The time resolution calculated from these expressions for the detector without the light guide was 1.39 ns. After incorporating the light guide, however, we got 1.01 ns as a time resolution for the detector. The improvement of about 30% in the time resolution for the detector with the light guide is an indication of better light collection after incorporating the light guide.

Annand et al.,[32] has measured the time resolution for several NE213 scintillators having different diameters and different thickness. According to his results, a time resolution of about 0.7 ns is expected for a 10"diamx4"thick scintillator. This is about 30% less than the value we have. This deviation could be due to the different thickness and different photomultiplier used in their detector. It is also known that an improvement of up to 21% can be achieved in time resolution if one uses dynode signal instead of anode signal[33]. In this experiment, the anode signal was used for time resolution measurement.

3.3. PULSE SHAPE DISCRIMINATION TEST

The time course of the light intensity as well as the integrated light output from some scintillators when excited by gamma rays are different from those when excited by neutrons. Such a difference results in unequal risetimes in the two cases at the output of the photomultiplier coupled to the scintillator. Neutrons which are detected through recoil protons are found to yield a longer risetime than that due to gamma rays. This variation in risetime is often exploited to discriminate between neutrons and gamma rays in PSD[34].

A number of methods of PSD have been developed utilizing the relative difference in the magnitude of the fast and the slow components in the light pulse. However, when the experimental system is required to operate over a large range of neutron energies, the best PSD is provided by the zero-crossover (ZC) technique. If the pulses from a scintillator photomultiplier combination are integrated, the risetime of the integrated pulses will be different depending upon whether they were produced by electrons (gamma rays) or recoil protons (neutrons). Since the risetimes differ, a double differentiation of the integrated pulses produces baseline crossover points that are amplitude invariant functions of the respective rise times. A measurement of the time difference between the delayed anode current pulse and the ZC point of the double differentiated pulse uniquely determine the type of the particle[35].

Several types of discriminators were designed to process the risetime distribution. Generally they can be classified into two categories , namely the Zero Crossing[36] and the Leading Edge[34]. Both types of the discriminators generates the pulse shape risetime distribution spectrum which consists of two peaks corresponding to gamma rays and neutrons .

Conventionally a zero crossing PSD spectrum is characterized by two parameters , a figure of merit M and the neutron peak-to-valley ratio ,P_n/V[35]. The figure of merit M is defined as the separation between the centroids of the gamma and the neutron peaks divided by the the sum of their FWHM ,

$$M = \frac{C_n - C_\gamma}{FWHM_n + FWHM_\gamma}$$

It was proved experimentally[36] that a 100% discrimination is reached if M has a value of 1.5 or more.

3.3.1. Experimental Procedure

In this experiment , a zero crossing PSD module designed by Sperr et al.[37] was used. Inside this module, the time signal, the anode signal of the 10" scintillator, is fed into a preamplifier where it is integrated and differentiated. This will result in a separation of the signals having different risetime. The signal is then fed into a high-gain limiting amplifier. This is used to enhance the

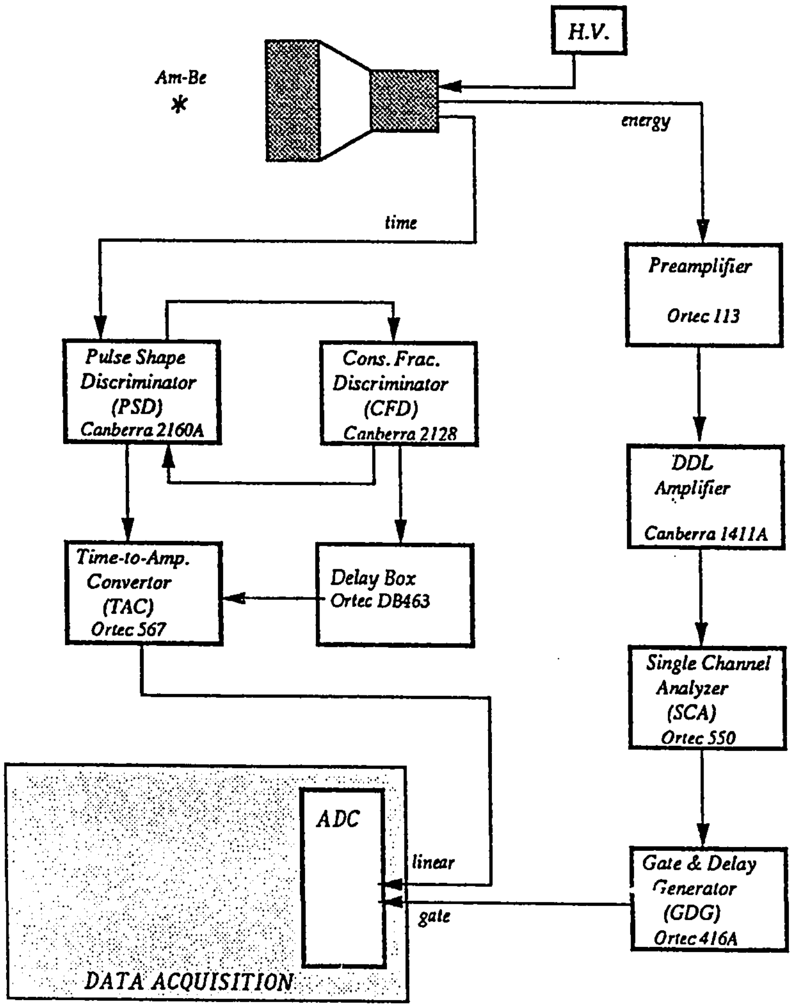

Fig.3.11 Schematic diagram of the electronics used in the PSD test.

separation between the two signals. A gate is generated if a triggering signal (strobe) is placed between the crossing points of gamma rays and neutrons, allowing only neutrons to be counted.

The neutron source used in this test was a 350 μCi Am-Be source filtered by a 3 mm sheet of lead in order to reduce the intense gamma rays. ^{241}Am is an alpha particles emitter usually used to bombard ^{9}Be by alpha's to get neutrons according to the eq.

$$^{9}\mathrm{Be} + \alpha \rightarrow {}^{13}\mathrm{C}^{*} \rightarrow {}^{12}\mathrm{C}^{*} + \mathrm{n}$$

deexcitation of ^{12}C produces a 4.4 MeV gamma rays.

As shown in fig.3.11, the anode signal of the 10" scintillator is fed to a CFD module through the PSD module. One of the outputs of the CFD was used as a strobe to trigger the PSD . The other output was fed to a TAC as a start signal. The output of the PSD unit was used as a stop signal for the TAC. The TAC output was digitized by an ADC which was hooked to the ERL data acquisition system. The spectrum generated represent the rise time distribution of the neutrons and the gamma rays . Fig. 3.12 shows a typical PSD spectrum.

The performance of PSD module strongly depends upon the input count rate. For certain input-frequency, it gives the best performance. This frequency has to be determined experimentally. In order to do this P_n/V was measured at fixed energy bias as a function of strobe frequency. Fig.3.13 shows the neutron peak-to-valley ratio as a function of strobe signal frequency for two different

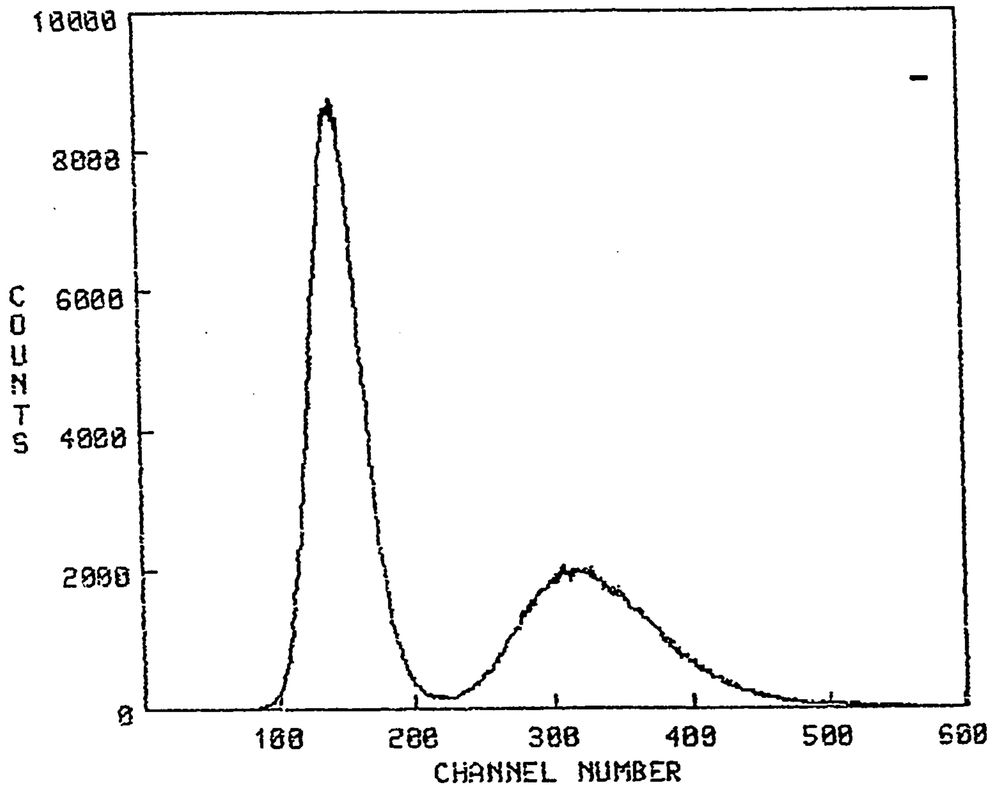

Fig.3.12. A typical PSD spectrum.

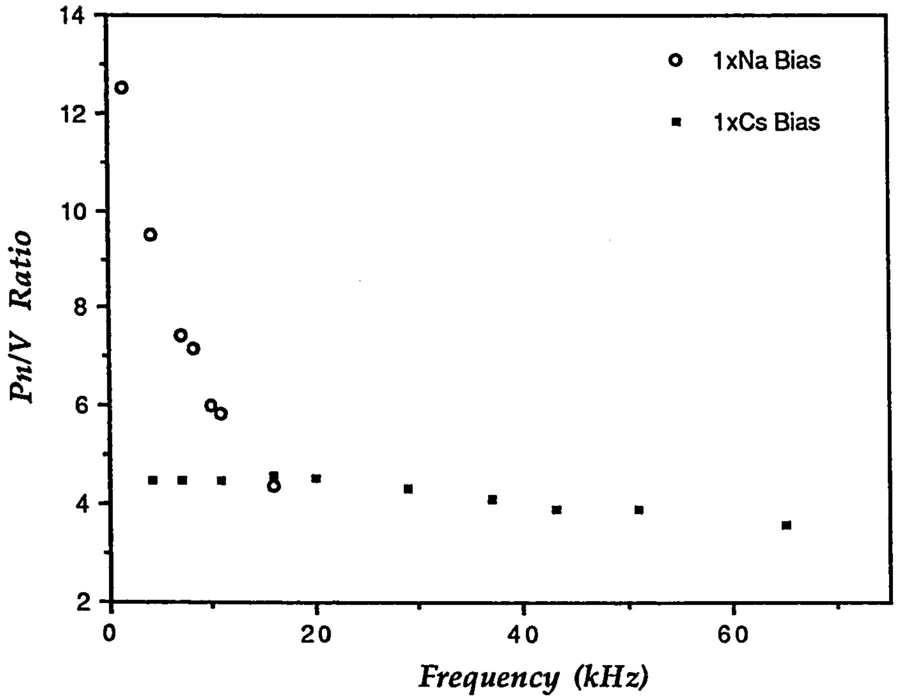

Fig.3.13. Effect of the strobe frequency on the PSD performance

biases. The P_n/V ratio improves as the strobe frequency decreases till it reaches saturation level. one can choose the operating frequency of the PSD module on the saturation plateau of P_n/V. For this test, a frequency of 1.5 kHz was chosen for the rest of the experiment.

After determining the optimum frequency of the input signal to the PSD module, the effect of energy bias on PSD parameter was studied. In order to set the energy bias, TSCA lower level was calibrated in terms of energy. P_n/V ratio and the figure of merit M were measured for energy bias range from 0.2 to 1.2 MeV.

3.3.2. Results and Analysis

In general, the P_n/V ratio and the figure of merit M increase with increasing the bias. The results showing the dependence of the PSD performance on the energy bias are tabulated in table 3.7. The detector without the light guide shows a slightly better performance than with the lightguide. In this case , the P_n/V ratio reaches saturation at a bias of about 1.0 MeV. At this bias the value of M is only about 1.15. This is about 80% of the 1.5 value at which 100% discrimination could be reached. Within the experimental uncertainties, the value of M for the detector with the light guide at this bias is about the same, M=1.12. However, the P_n/V ratio decreases from 30% less than that without the light guide at low biases to 10% at the highest bias. This deterioration in PSD performance after incorporating the lightguide is because those neutrons which

TABLE 3.7

Effect of light guide on the PSD performance

Electron Energy	P_n/V		M	
(MeV)	without LG	with LG	without LG	with LG
0.278	4.25	3.10	0.900	0.864
0.516	8.29	6.31	1.030	0.891
0.785	12.51	8.69	1.120	1.069
1.032	13.18	10.96	1.150	1.120
1.155	14.01	12.38	1.190	1.160

were not counted without the light guide because of non-uniform light collection are now counted. These neutrons add to both the peak and the valley and hence increase the P_n/V ratio.

CHAPTER FOUR

NEUTRON DETECTION EFFICIENCY MEASUREMENTS

Energy resolution and time resolution are important parameters in efficiency measurements based on the Time-of-Flight method. Accurate determination of the energy of the particle is needed in setting the efficiency bias. Also, knowing the time of arrival of a particle exactly reduces the error in calculating the neutron energy. As was shown in the previous chapter, incorporating a light guide improved these two properties of a scintillator. Therefore, efficiency measurements of the 10" scintillator could be carried out with a high degree of precision.

4.1. EXPERIMENTAL TECHNIQUE

4.1.1. General Considerations

The Time-of-Flight (TOF) technique utilized in these measurements is one of the best methods used for determining the energy of prompt neutrons emitted by spontaneous fission sources. The essence of this method is to measure the time a neutron takes to travel a distance L between the neutron source and the detector. Knowing the neutron velocity ,v=L/t , the energy can be calculated using either the relativistic expression

$$E = Mc^2\left(1/\sqrt{1 - L^2/c^2t^2}\right)$$

or the non-relativistic expression

$$E = \tfrac{1}{2}Mv^2$$

depending on the neutron energy range and the resolution of the experiment. The energy resolution depends on the time resolution, as $(\Delta E/E)=(2\Delta t/t)$, if the uncertainty in measuring the flight path L is made negligible by increasing L.

The measurement of the time of arrival of a neutron is usually accomplished by means of a detector counter telescope consisting of two detectors placed a distance L apart. The detector setting close to the neutron source is used to provide a start signal to a Time-to-Amplitude Convertor (TAC). This signal could have resulted from a gamma ray or from a neutron. The TAC stop signal is provided by the other detector, and also could be caused by a gamma ray or a neutron. The TAC spectrum resulted shows two peaks, a sharp peak corresponding to gamma rays and a broad peak corresponding to neutrons with different energies. Since gamma rays travel at the speed of light, the actual time of the arrival of the gamma ray can be calculated from , t=L/c. If the spectrum is calibrated so that time per channel is known, then the time of the arrival of the neutrons of different energies can be found, and therefore the energy can be calculated.

4.1.2. Equipment

The detection system used in these measurements consists of two NE213 liquid scintillators. The first is the detector whose efficiency to be measured, the 10" scintillator. The second is a fast 2" diameter x 2" thick (50 mmx50 mm) NE213 scintillator, used as a reference to detect the start of an event. The detectors are connected to a large number of electronic modules divided into three branches : the pulse-height branch, the TOF branch and the PSD branch. The pulse-height branch is used to record energy signals in the 10" detector originating from recoil protons. It consists of a preamplifier, and a DL amplifier. The TOF branch is used to record the time difference in the arrival of two signals coming from the two detectors. It consists of two Constant Fraction Discriminators (CFD), a Delay Box and a Time-to-Amplitude Converter (TAC). The PSD branch, is used to discriminate between the neutrons and the gamma rays. It consists of a PSD module, a Delay Box, a TAC and one of the TOF branch CFDs. A Linear Fan-Out module is used to generate three output from one CFD inputs.

Since coincidence condition from the three branches must be reached, a Coincidence Unit is used. A gate is generated from the pulse-height branch by using a Single Channel Analyzer (SCA) and a Gate and Delay Generator (GDG). The three linear outputs of the three branches go through Linear and Gate Stretcher (LGS) modules where there widths are adjusted and then fed into the first electronics in the Data Acquisition system (which will be discussed in section 4.1.3) the Analog-to-Digital Converters (ADC). The electronics in the three branches explained above are shown in fig.4.1 in operation set-up.

4.1.3. Three-Parameter Data Acquisition

The need for a multiparameter data acquisition arises in the study of events in terms of more than one parameter. The usual manual way to do this is by recording one parameter using a recording system while the other parameters kept limited by a Single Channel Analyzer SCA. After having adequate counts, another parameter is recorded and the others are fixed.

The ERL facility offers a multiparameter data acquisition system in which the parameters of an event are recorded simultaneously on a magnetic tape and sorting of these tapes with the required conditions is done via software. References 27, and 28 provides more information about the multi-parameter data acquisition system at ERL.

In our experiment, the event is represented by three parameters, namely the pulse-height signal, the pulse shape discrimination signal and the time-of-flight signal. As shown in fig.4.2, the three linear signals are delayed and their widths are controlled using a set of three Linear Gate Stretcher LGS modules. The outputs of these modules are fed into corresponding Analog-to-Digital Converters ADCs to be digitized. On the other hand, the coincidence gate pulse is used to produce the three-parameter gate of variable width through a Router-Gate module. The output of this module is applied to the gate inputs of the three

ADCs. The gate should encloses the three linear pulses to ensure no further input pulses are converted until all the data has been read by the MBD.

Only one signal is required to interrupt the MBD for reading the multi-parameter data and transferring it to the VAX. The requirement for this signal is that it becomes active only one data is ready at the outputs of the ADCs taking part in the acquisition process. This could be a LAM signal from the ADC acquiring the last arriving signal. This LAM signal will then represent the whole signal, while the otherLAMs from the other ADCs do not affect data acquisition. For this reason the energy signal coming from the amplifier was delayed from the other two signals by the LGS module. This ensures that this signal will not be processed until the others were completely processed. The PSD and TOF signals were made to arrive simultaneously, and 1ms after the gate, in order to reduce dead time. The pulse-height signal starts 0.8 ms after the end of the two other signals. Fig.4.3 shows a typical time correlation of the three signals used in this experiment.

4.1.4. Neutron Source

A ^{252}Cf isotope was used as a neutron source in these measurements. This source has some advantages over other sources. It was studied thoroughly[8] and found that it has a well defined neutron spectrum. The last published data showed that the experimental neutron spectrum resulting

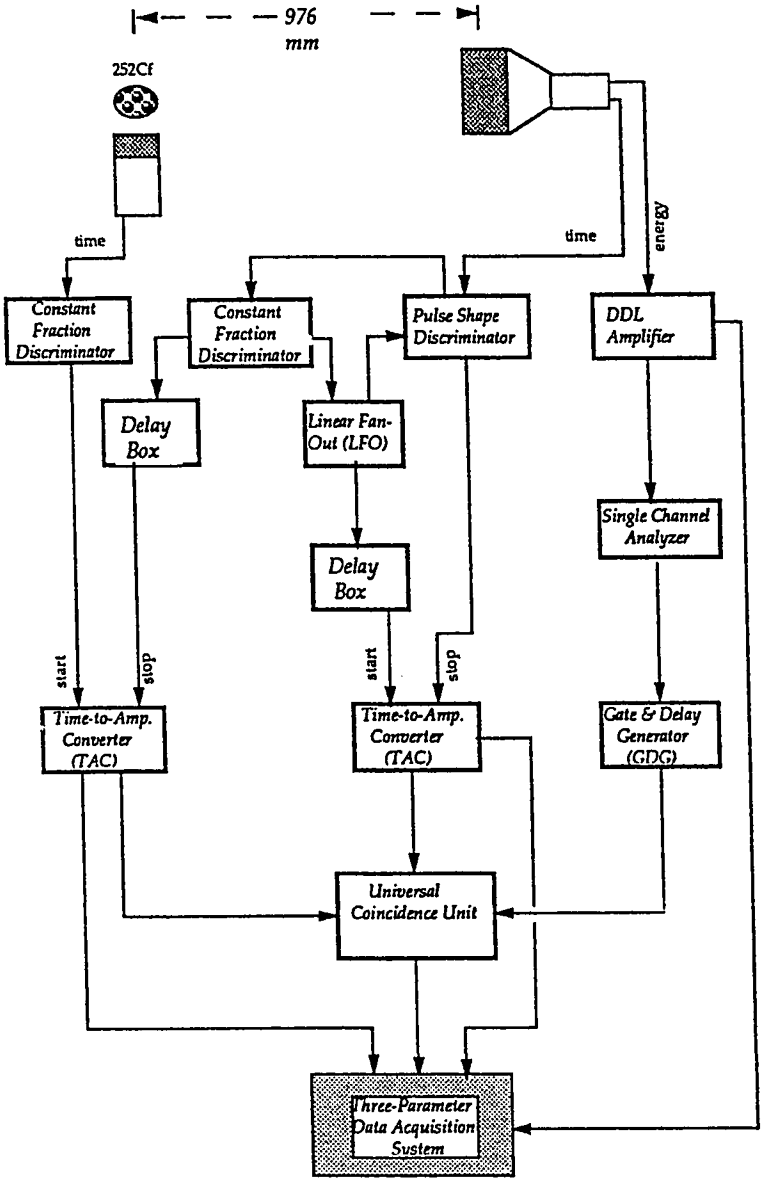

Fig.4.1. Schematic diagram of the electronics used in the the Time-of-Flight measurements

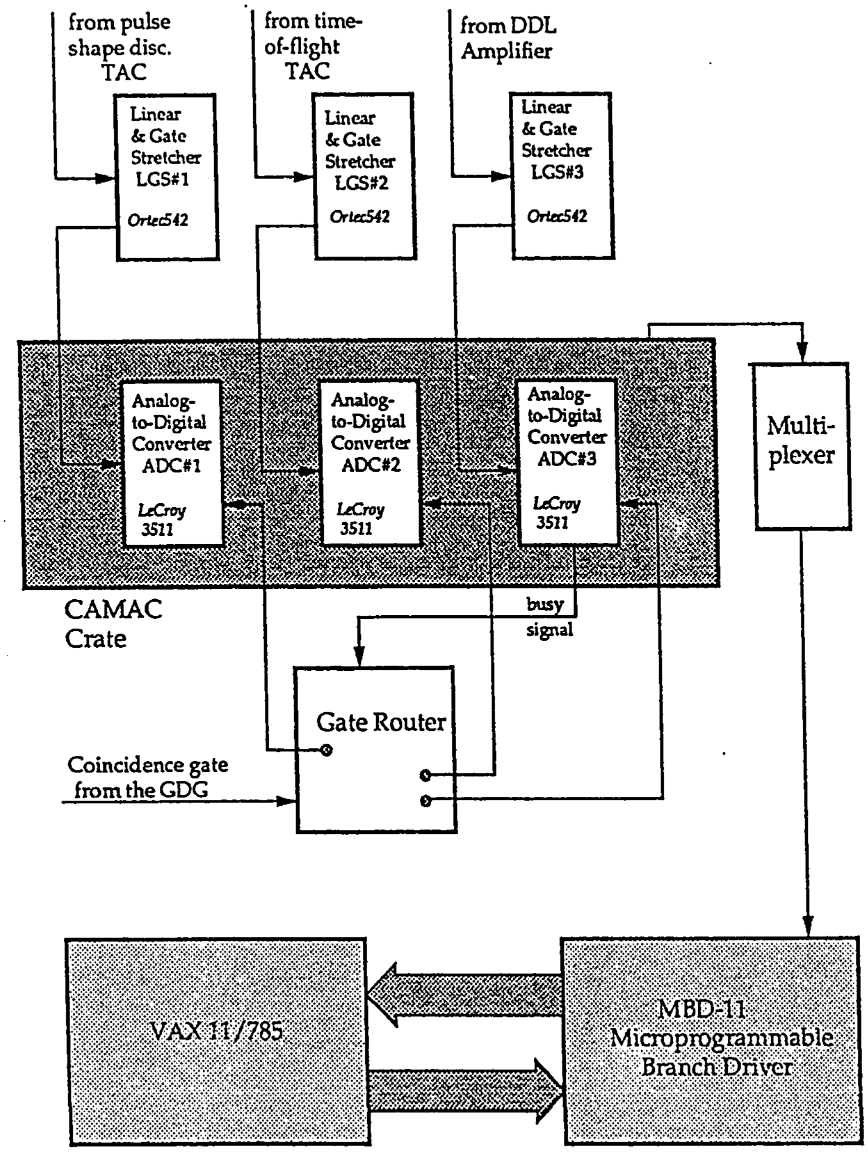

Fig.4.2. A block diagram showing the different units involved in the three-parameters data acquisition system.

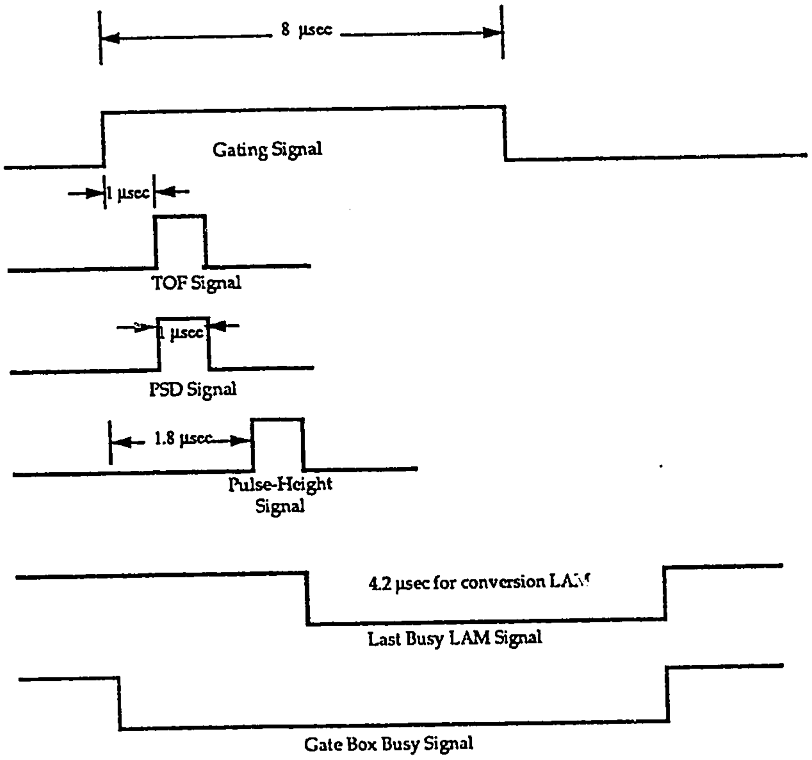

Fig.4.3. The correlation between the TOF signal, PSD signal, and the Pulse-Height Signal.

from fission process can be best described by a Maxwellian distribution[38]

$$n(E) = c\sqrt{E}\exp(E/E_o)$$

with temperature kT= E_0= 1.355 MeV. The experimentally measured multiplicity of the ^{252}Cf is v= 3.77. It emits 2.311×10^{12} neutrons by spontaneous fission. It has a half-life of 2.646 years. It is the only known radioisotope that can be fabricated into small-sized sources that emit neutrons intensely over a practical period of time.

^{252}Cf decays by both alpha emission and spontaneous fission. One spontaneous fission occurs for every 31 alpha emissions and produces 3.77 neutrons. The spectrum of the fission neutrons emitted by th ^{252}Cf is shown in fig.4.4. The neutron energy has a maximum at about 1.0 MeV and has an average neutron energy of 2.3 MeV. In these measurements the source is inscribed in a cylindrical can of radius 43 mm.

4.1.5. Procedure

In our measurements, the neutron energy distribution from the spontaneous fission of ^{252}Cf was studied using the TOF method. The 10"detector was placed 976 mm from the center of the box containing the ^{252}Cf source. The choice of this distance was to decrease the uncertainty in the flight path and hence improves the energy resolution. The reference detector was placed very close to the source (about 5 cm away) in order to minimize the time of arrival of the particles triggering the TAC. The two detectors were put in a 90 degree geometry so as to minimize background resulting from backscattering of particles from the reference detector and detected by the detector understudy. The time signals from the reference detector were used to supply the time-of-flight TAC with start signals after the time of the arrival of the signal was determined by a CFD. The 10" detector was used to provide the time-of-flight TAC with stop signals. In order to suppres the gamma rays (under the neutron peak), in the offline analysis, a PSD branch was added to the TOF circuit as shown in fig.4.1. The output of the 10" CFD was divided into two signals through a Linear Fan-Out (LFO) module. One of the LFO outputs was fed to a PSD module while the other was sent as a start signal to the pulse shape discrimination TAC after being delayed. The PSD output was the stop signal for the pulse shape discrimination TAC. The pulse-height signal from the 10″ scintillator was passed through a SCA module with fully opened window to produce a gate from a GDG module. The three gates produced, namely the time-of-flight TAC gate, the pulse shape discrimination TAC gate and the pulse-height GDG gate, were fed into a Coincidence unit. By doing this, only signals from the same event are recorded. A coincidence gate was then generated using a GDG module and stretched in time using a Dual Gate Generator (GDG) module. This gate along with the three linear signals were sent to the control room for data acquisition and analysis.

A typical TOF spectrum generated in these measurements is shown in fig.4.5. The spectrum shows TOF channels as abscise. In order to convert the channels into time, the TAC spectrum was calibrated using a Time Calibrator

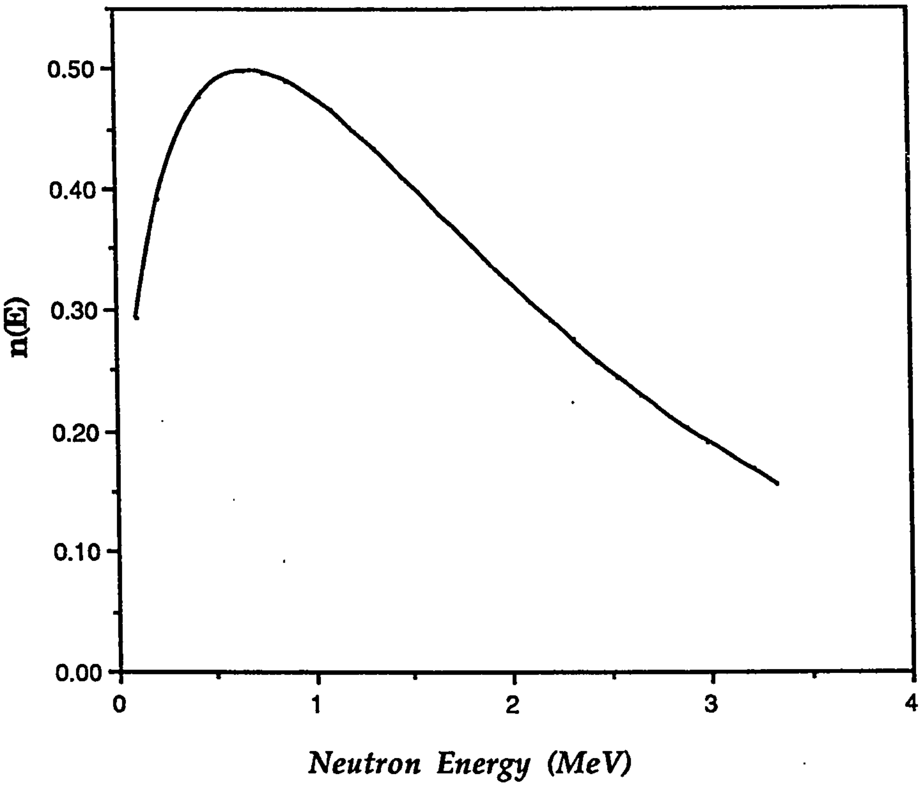

Fig.4.4. The maxwellian neutron energy spectrum of ^{252}Cf isotope at kT=1.35 MeV

Ortec model. The output of this module consists of equidistant spikes. The time separation between the spikes is known (preselected by the user) and therefore the time dispersion (sec/ch.) can be calculated. The energy calibration was being checked daily by measuring the edge of the ^{22}Na source.The total number of events recorded at the end of the 400 hours experimental run were 1.5x10^6 event.

4.2. DATA ANALYSIS

In addition to the TOF spectrum generated, two more spectra were generated representing the PSD events, fig.4.6, and the pulse height events, fig.4.7. In the TOF spectrum, fig.4.5, two main peaks exist ; a sharp peak representing gamma rays recorded by the TAC as stop signals, and a broad peak representing neutrons with different energies. The number of events under the gamma peak is twice that number under the neutron peak. The small peak, located to the left of the gamma rays peak, is a result of gamma rays induced by neutrons scattering from the floor. This peak is not of importance in our analysis. The PSD spectrum also shows two peaks. These peaks represent the risetime distribution of the gamma rays and the neutrons emitted by the ^{252}Cf source, without any energy bias. The ^{252}Cf source shows a poorer PSD performance compared to the Am-Be source. This is attributed to a higher gamma to neutron intensity ratio in the ^{252}Cf source than that of the Am-Be source. Lastly, the pulse height spectrum is a mix of neutrons and gamma rays detected by the 10" detector. For this reason, this

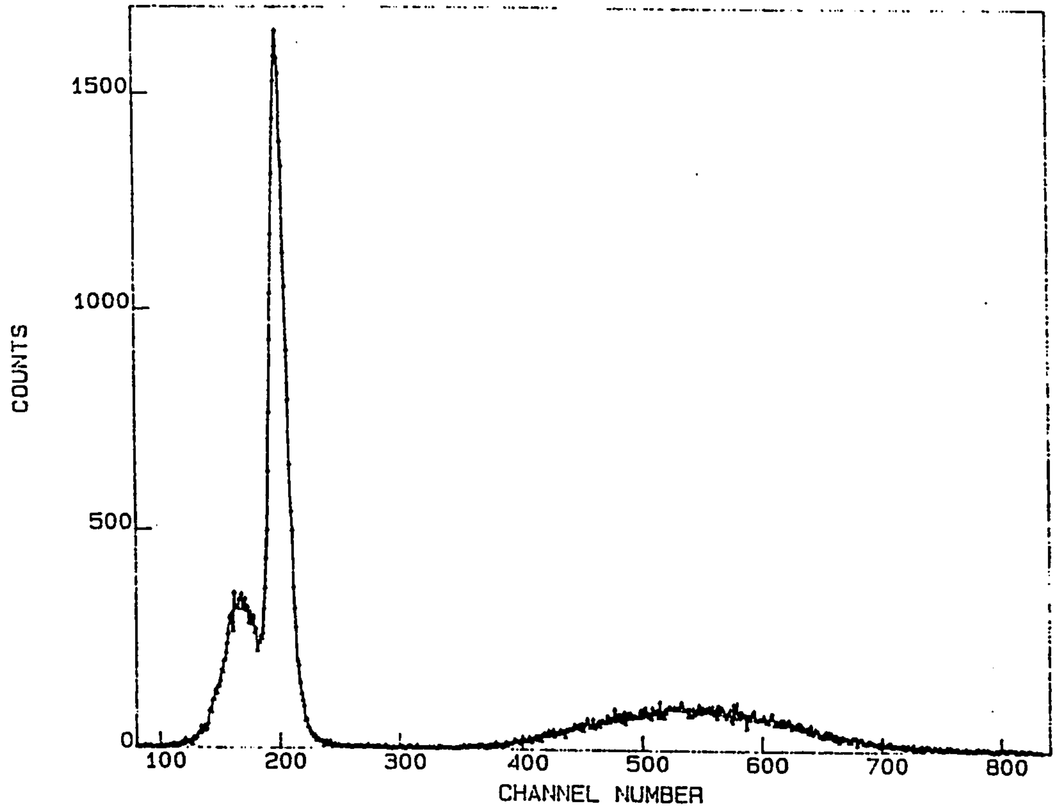

Fig.4.5. A typical Time-of-Flight spectrum showing the distribution of the time of arrival of the neutrons and the gamma rays emitted by the ^{252}Cf source

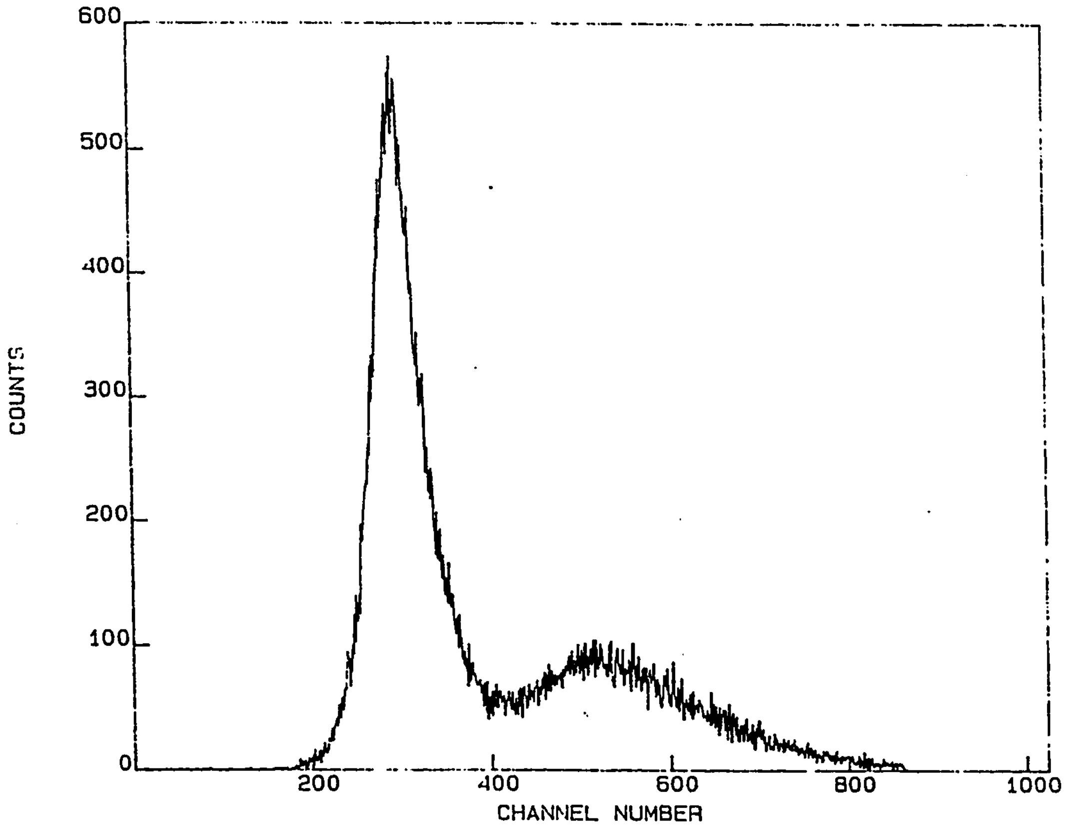

Fig.4.6. A PSD spectrum showing the risetime distribution of the neutrons and the gamma rays emitted by the ^{252}Cf source

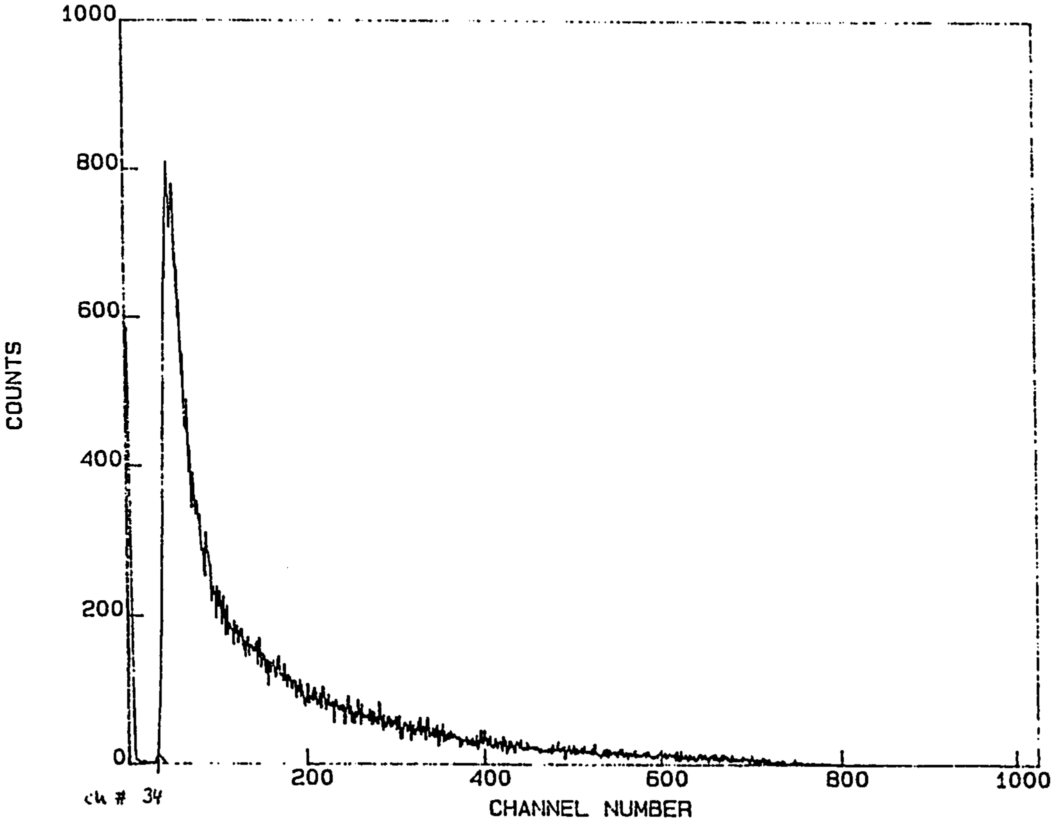

Fig.4.7. The pulse-height spectrum of the neutrons and the gamma rays emitted by the ^{252}Cf source

cannot be taken as the spectrum of the fission neutrons emitted by the ^{252}Cf source. All the information needed for the extraction of the response function and the efficiency curve are in the TOF spectrum. Therefore, analysis of the TOF spectrum is the first step to reach desired results. The PSD spectrum will be used to suppress the gamma rays in the TOF spectrum.

4.2.1. Analysis of the Time-of-Flight Spectra

The analysis of a time-of-flight spectrum means the transfering of the TOF spectrum into an energy spectrum. This energy is calculated by measuring the absolute time of flight of neutrons over the given distance. As the time of flight contains the gamma peak, it allows the calculation of the neutron flight time relative to the gamma rays. This time can then be converted into absolute time of flight of neutrons from the known gamma flight time. This procedure involves several steps,i.e., time calculation of TOF spectrum, determination of separation of the gamma peak and each neutron TOF channel, calculation of the absolute flight time of neutron and finally, calculation of the energy of each TOF channel.

The centroid of the gamma peak in our TOF spectrum was located at channel no. 149. This correspond to a time of $t_\gamma=L/c$. Therefore, the time a gamma ray took to cover this distance L was 3.25 nsec. The relative time between the arrival of the gamma rays and a neutron, $T_{n\gamma}$, given in channels, was converted into absolute time using the value of the time dispersion given by the

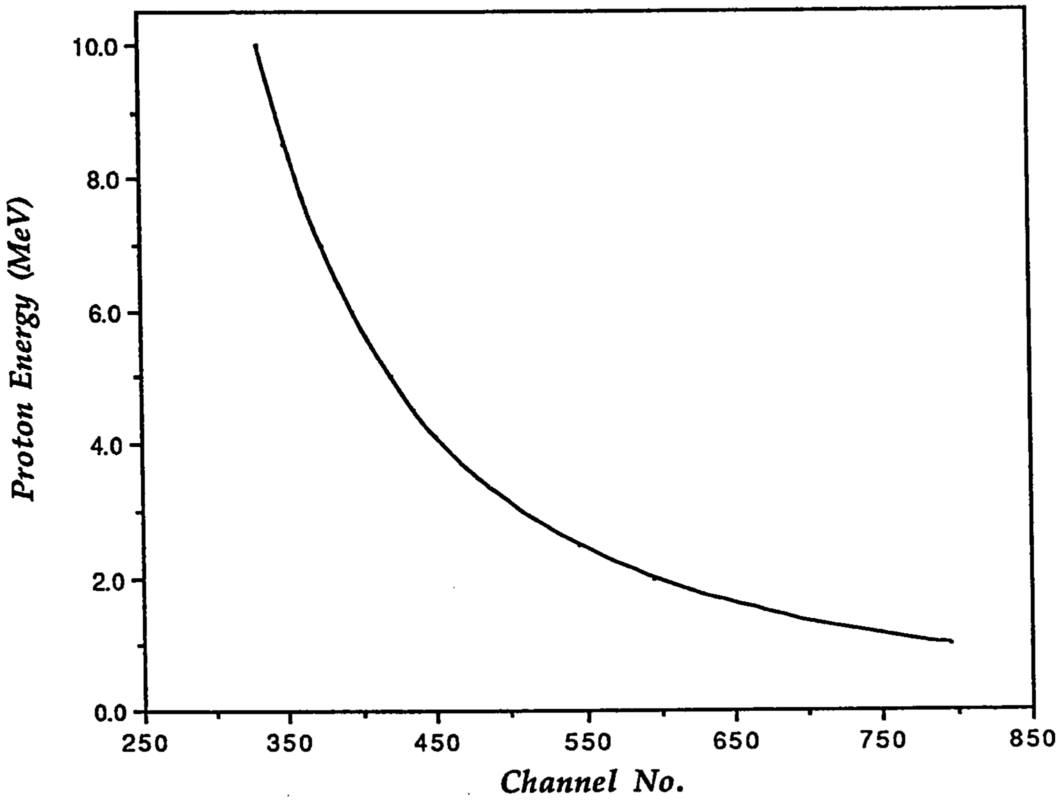

Fig.4.8.A curve showing the relation between proton energy and the TOF channel no.

time calibrator and equals 104 psec/channel. Adding $T_{n\gamma}$ to t_γ, the absolute time, tn, of the arrival of a neutron was calculated. The velocity of this neutron was then calculated using $v=L/t_n$. Since the neutrons emitted by the ^{252}Cf source have maximum energy of about 10 MeV << Mc^2, the non-relativistic expression for the energy was used to find the neutron energy.

A computer code, CALENER (Appendix), was written to do all these calculations for the whole neutron energy range. The result was a curve relating channels to energy of the neutrons in the TOF spectrum. This curve is shown in fig.4.8. The response function and the efficiency measurements are dependent on the information given by this curve.

4.2.1.a. Response Function:

Response function is basically a correlation of detector light output for electrons and protons . As response function measurements were carried out with ^{252}Cf source which emits a continuous spectrum of neutron energy range from 0.3 to 10 MeV, producing monoenergetic neutrons is necessary to get the pulse height spectrum. In order to select monoenergetic neutrons, TOF spectrum was acquired and gates were chosen on the spectrum to select the bins of neutron energy. The detector pulse height spectrum was acquired as a function of TOF gates for several neutron energies. Gamma rays were suppressed in the pulse height spectrum by adding a second set of gates selected of the neutron peak of the

PSD spectrum.

This was made by first sorting the tape with the appropriate PSD gates set on the TOF spectra via software and adding the resulting spectra to each other. After that, energy bins of 50 keV width were set on the neutron peak of the TOF spectrum, using the relation found between channel no. and the proton energy. The counts in each bin were then integrated and diffused neutron edges were produced. The channel no. of half the height of the edge is conveniently taken as to correspond to the proton energy preselected. Using the electron energy calibration done with the gamma sources, ^{137}Cs, ^{54}Mn and ^{22}Na, the electron energy corresponding to this channel no., or proton energy, can be extracted. This gives a relation between the proton and the electron energies, having the same light output. The steps discussed above are shown in fig.4.9a-d. For the sake of comparison with published data, two schemes of calibration were used : coincidence peak and Compton edge schemes. Fig.4.10 shows the two calibration schemes used. The experimental data of the response function are plotted as shown in fig.4.11 for the two calibration schemes. They were fitted to the following expressions

$$E_P = -5.20\times10^{-2} + 0.271E_e + 2.62\times10^{-2}E_e^2 \quad ...(A)$$
$$E_P = -6.34\times10^{-2} + 0.311E_e + 3.01\times10^{-2}E_e^2 \quad ...(B)$$

where eq. (A) refers to the coincidence peak energy calibration scheme and (B) to the Compton edge calibration. Table 4.1 shows a comparison of present data with other published data by Gul et al.[11], Cecil et al.[39] and Batchelor et al.[40]. For there measurements they used scintillators with sizes, 5"x5", 2"x21/2"all of the

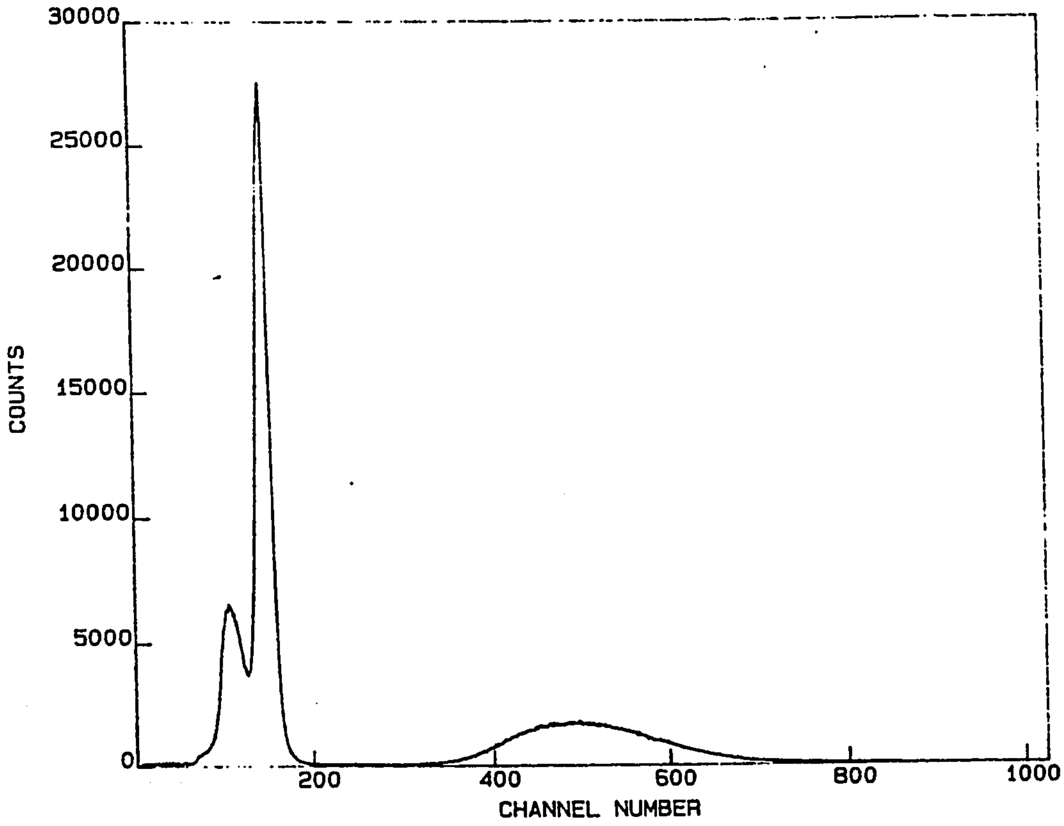

Fig.4.9a. The added TOF spectrum showing the total number of gamma and neutron events recorded in this measurements

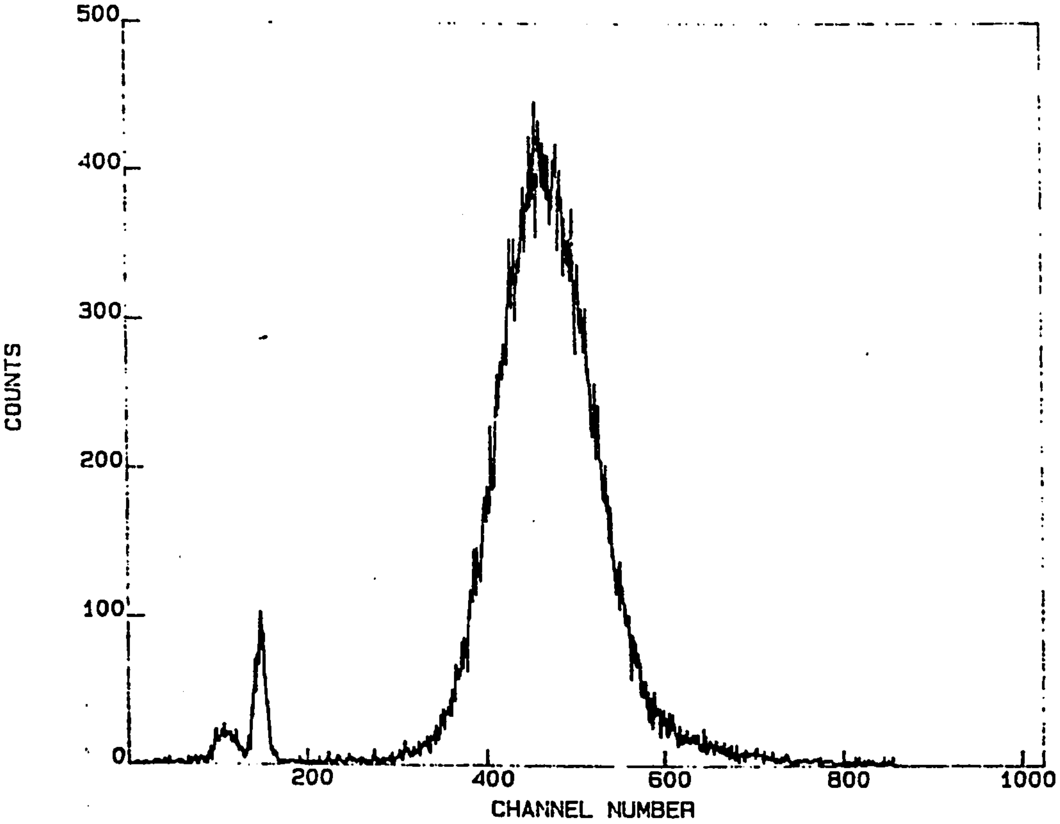

Fig.4.9b. The TOF spectrum after applying PSD gates to suppress gamma rays

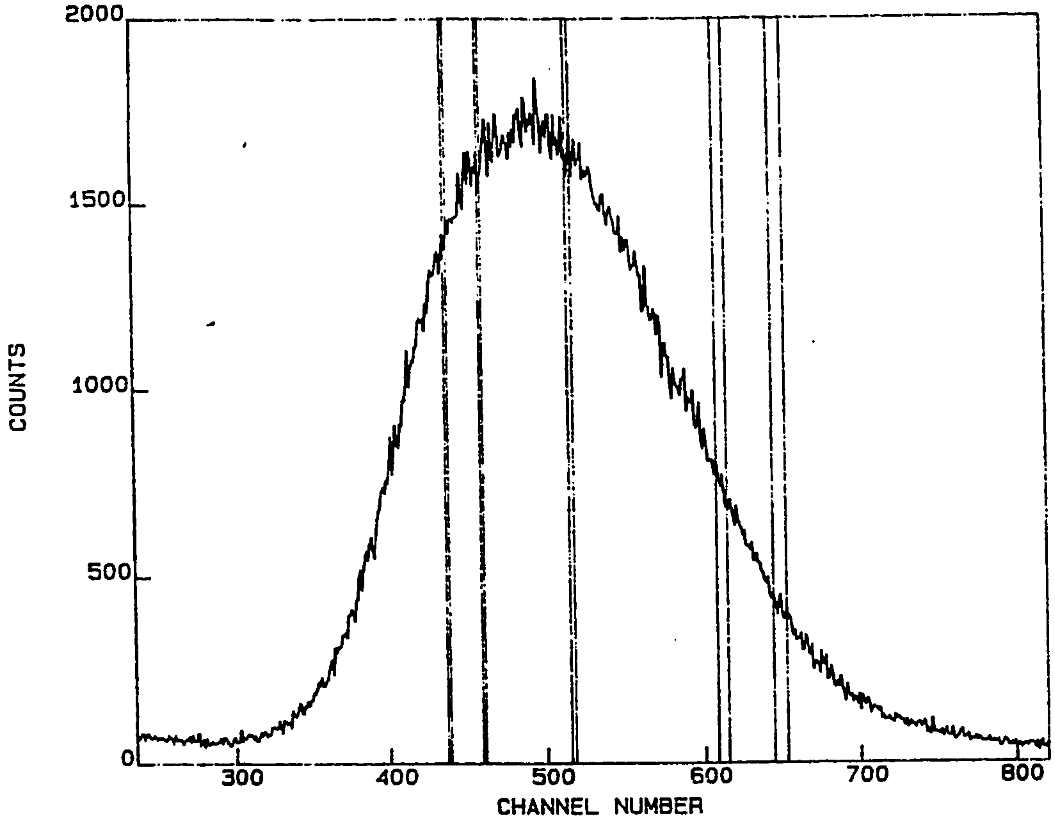

Fig.4.9c. Energy gates are set on the neutron peak in the TOF spectrum

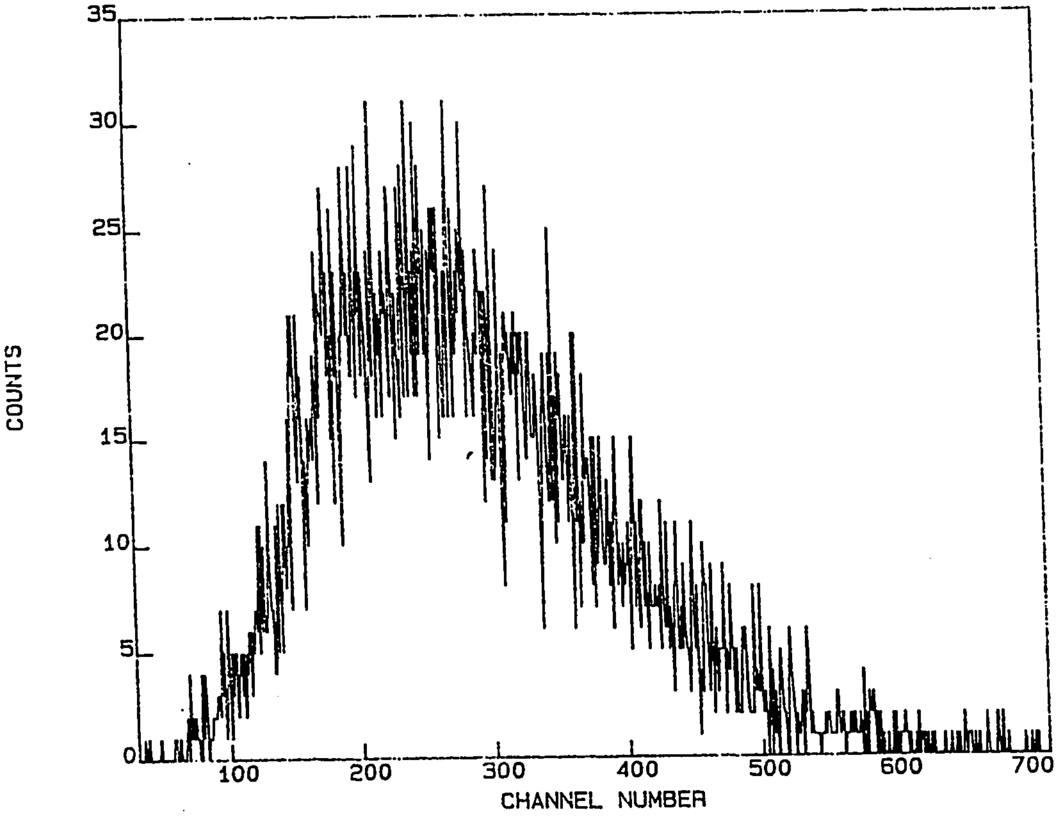

Fig.4.9d. The proton-recoil pulse-height spectrum resulting from integrating the counts in each energy bin

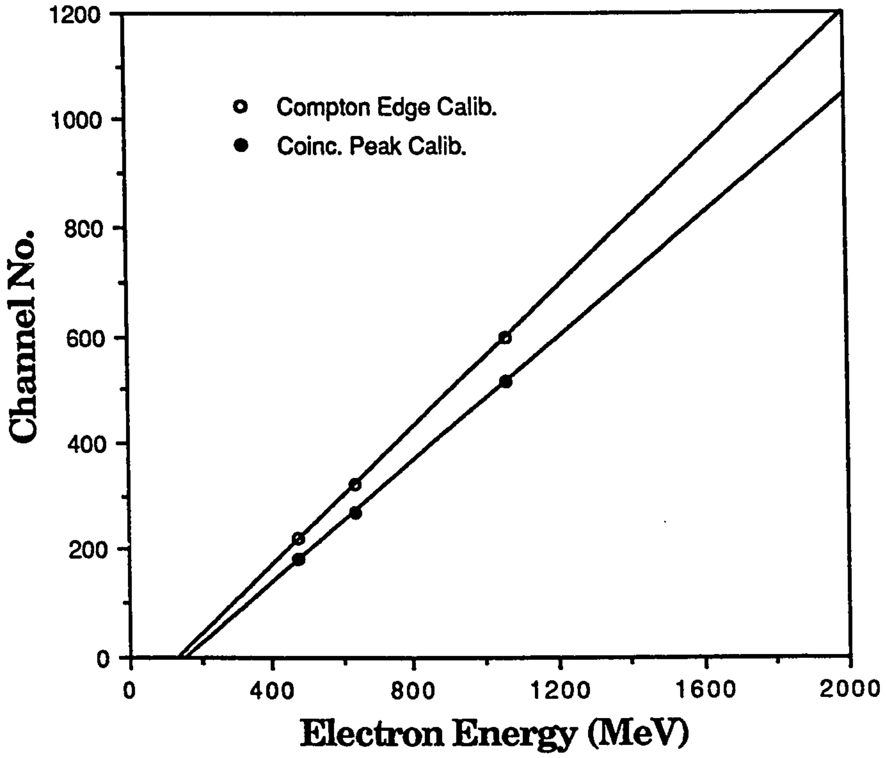

Fig.4.10. The two calibration schemes taken with ^{137}Cs(0.477 MeV), ^{54}Mn(0.639 MeV) and ^{22}Na(1.062 MeV) gamma sources

TABLE 4.1

Comparison of the present measurements of the response function of the 10" scintillator with previously reported data.

Proton Energy (MeV)	Electron Energy (MeV) Present Work-A	Gul et al.	Batchelor et al.	Cecil et al.
1.000	0.245	0.213	0.234	0.206
1.500	0.413	0.393	0.386	0.384
1.750	0.502	0.488	0.462	0.484
2.000	0.595	0.586	0.542	0.591
2.500	0.789	0.792	0.713	0.824
2.750	0.891	0.900	0.803	0.949
3.000	0.997	1.011	0.897	1.078
3.500	1.217	1.243	1.095	1.350

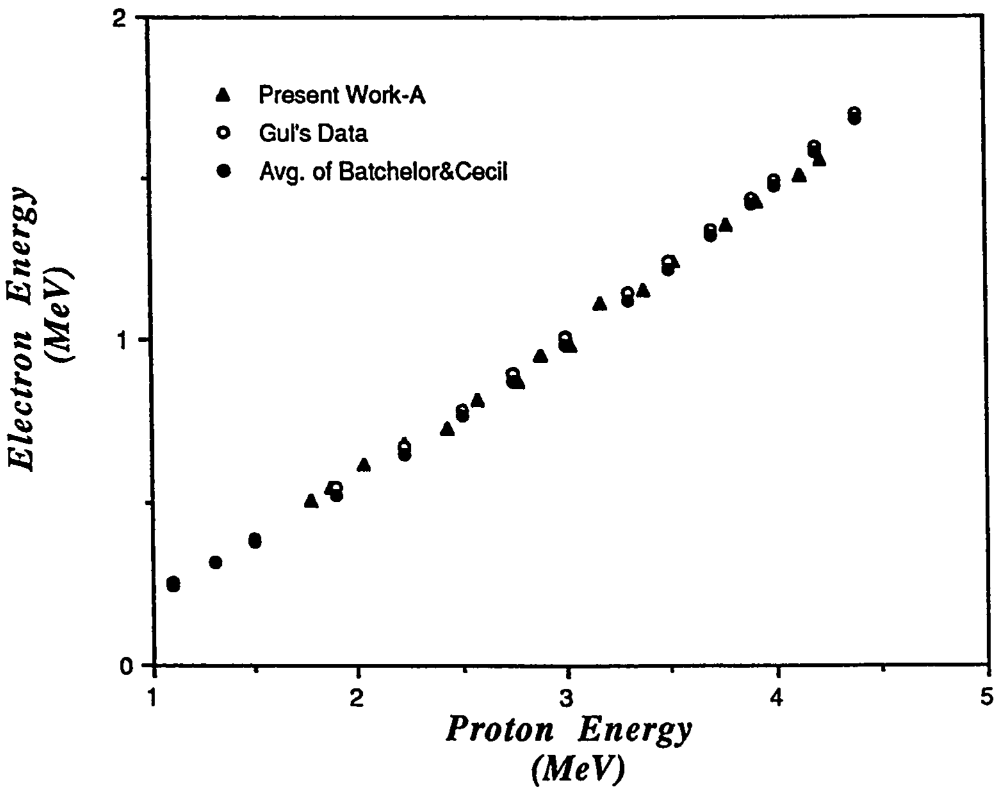

Fig.4.12. Present data of the response function plotted along with other reported data.

NE213 type. The agreement between present data with Gul data is obvious. The deviation between the present data and Gul's data is less than 3% for most of the points. Also it can be inferred from the table that at high proton energy the other two sets of data by Cecil and Batchelor deviate from each other but their average come close to present data. Fig.4.12 shows data of the response function found in the present work, Gul work, and the average of Cecil and Batchelor. They almost lay on the same curve. This agreement is expected since the response function does not depend on the size of the scintillator[7]. The small deviations in these sets of data, however, is expected also since other factors, such as history and manufacturing of the scintillator have some effects on the response of the scintillator. Also the uncertainty in the determination of the energy through the half-height position which is dependent on the resolution of the detector could contribute to this deviation in the different data.

As one can see, the maximum proton energy given in table 4.1, 3.5 MeV, corresponds to the maximum electron energy, about 1 MeV, used in the calibration. In order to look for correlation at higher proton energies, gamma ray sources with higher energies should be used in the calibration process. When the 4.4 MeV gamma rays of the Am-Be source were used, it showed a non-linearity in the response of the scintillator at this high energy. This non-linearity was attributed to air bubbles inside the scintillator due to aging effects.

4.2.1.b. *Efficiency Measurements:*

Efficiency curves were generated for different energy biases. These biases were set by choosing gates, via software, open at one end(ch. no. 1024). The other end was selected using the information given from the response function and the channel no. vs. proton energy curve. These gates were applied to the pulse-height spectrum. The effect of the energy gates is shown in fig.4.13. After that, PSD gates were also set as in the response function. The experimental points of the efficiency curve were chosen by selecting energy bins on the TOF spectrum. The width of each bin was 50 keV. The code CALENER was used to find the number of counts in each energy bin. For the same energy the corresponding counts in the standard spectrum of the ^{252}Cf source were calculated. When dividing the experimental number of counts by the standard ones, the points of the efficiency curve were generated. The background due to gamma rays under the neutron peak in the TOF spectrum not cut by the PSD gates was then subtracted. In TOF measurements two type of background always considered: The time independent background and the time-dependent background. The time-independent was calculated by averaging the flat region between the gamma peak and the neutron peak in the TOF spectrum. The time-dependent was calculated using the following expression

$$B(j) = S(j)[1 - \exp - kt(j)],$$

where B(j) is the time-dependent background in channel j. k is a constant determined by taking the average of the counts in channels covering a 50 keV energy width about the position that corresponded to the neutron detection efficiency. The time-dependent factor is t(j)=jdt, the channel j multiplied by the time desperion, in this case, dt=0.104 ns/Ch. S(j) is the sum of the counts in all the channels starting from zero until channel j.

The neutron detection efficiency curves of the 10" scintillator for two energy biases, 1.25 MeV and 2.00 MeV proton energy are shown in fig.4.14. For the first bias, the efficiency reaches a maximum of about 37% at a proton energy of about 4.30 MeV. Then decreases to 22% at a proton energy of about 7.00 MeV. For the 2.00 MeV bias, however, the maximum efficiency found was about 25% at about the same proton energy as for the first bias. The efficiency decreases to about 14% at a proton energy of about 7.00 MeV. The non-smotheness of the curve at a proton energy of about 5.50 MeV is due to scattering of neutrons with carbon nuclei. This could be due to the deexcitation of the first excited state of carbon $^{12}C(n,n')^{12}C^*$. Also above 6.00 MeV there is another structure which might be due to the reaction $^{12}C(n,a)^9Be$.

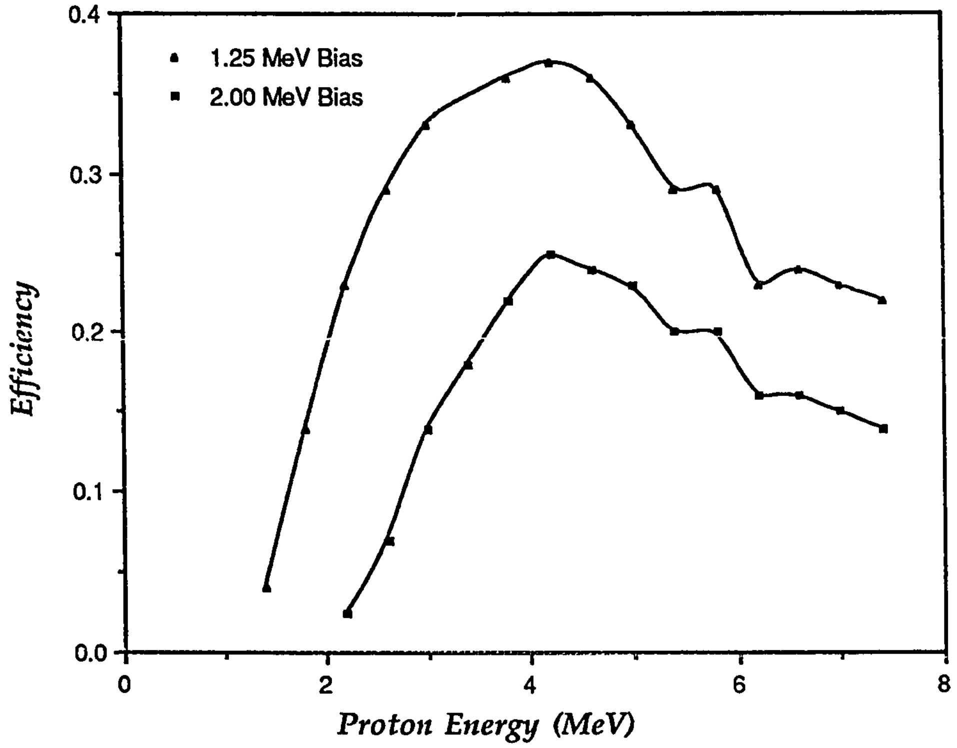

Fig.4.14. Efficiency curve of the 10" scintillator at two different biases

CHAPTER FIVE

SUMMARY AND CONCLUSION

In this project, a large 10" NE213 liquid scintillator directly coupled to a small 5" photomultiplier is to be used in neutron experiments where high count rate is necessary. This detector was modified by incorporating a plexi-glas conical light guide between the scintillator and the photomultiplier in order to collect the light from all points in the scintillator efficiently. This light guide was first partially coated with NE560 reflector paint so as to reduce the locus-dependent effects and hence to improve the detector resolution.

Several tests on the performance of the modified detector were carried out. Energy resolution tests were carried out utilizing the Gamma-Gamma coincidence technique and using standard gamma ray sources having energies in the range of 0.3 to 1.0 MeV. The results showed an improvement of 50% better than the original detector configuration. The results were also found to agree with published data. Time resolution tests wre also carried out utilizing a time coincidence technique and using a ^{60}Co gamma ray source. An improvement of about 30% were achieved.

The PSD (Pulse Shape Discrimination), however, deteriorated. At low energies, this deterioration is about 30%. At higher energies (more than 1.0 MeV

TABLE 5.1

Effects of the light guide on the performance of the 10" detector

Property	Electron Energy(MeV)	without Light Guide	with Light Guide	Effect
Energy Resolution	0.639	61%	28.5%	53% improvement
Time Resolution	0.500	1.39 ns	1.01 ns	28% improvement
PSD(Pn/V)	1.155	14.01	12.38	11% deterioration

electron energy) where most experiments are done, this deterioration decreases to about 10%. Table 5.1 shows the effects of the light guide on the energy resolution, time resolution, and PSD properties of the detector at selecte energies. After that, the goal of this research, the neutron detection efficiency measurement of the 10" scintillator, has started. For this measurement, the Time-of-Flight technique was utilized. This powerful method is used to determine the energy of the detected neutrons, with reference to the time of arrival of gamma rays emitted by the same source. The correlation between the neutron energies and the maximum energies of Compton electrons used for calibration is always measured. In these measurements, this correlation, usually called the response function, was found to agree very well with publish data for electron energies not more than 1 MeV. Above this energy, non-linearity in the response of the detector to gamma rays. Bubbles inside the scintillator could cause this behavior. Using the measured response function, two energy biases, 1.25 and 2.00 MeV proton energy, were chosen to generate the efficiency curve. When compared with published data with smaller size scintillators, this scintillator has a higher efficiency.

For future work on this problem, several suggestions should be mentioned. First of all, the problem of the nonlinearity of the response of the scintillator to gamma rays, should be solved. This could be done by refilling the scintillator with NE213 liquid scintillator leaving no bubbles in. After that, a calibration is done with high energy gamma sources. If the response is found to be linear, then the response function in this case can be extended to proton energies higher than 6 MeV. This will give a good check on tha data and would make it possible to set energy biases for the efficiency measurement more than 1 MeV electron energy.

Other recommendations regarding the efficiency measurers is the possibility of using accelerator base neutron sources. These sources could provide neutrons with energies more than the maximum that the ^{252}Cf can give. Neutrons with 14 MeV can be given directly from the accelerator at the ERL. Other energies can also be provided using carbon and hydrogen targets. Finally, calculation of the efficiency is now possible using the different codes based on the Monte Carlo method. The efficiency curves obtained from these fits will fill in the gaps between the experimental points and will extend the curve to higher neutron energies.

APPENDIX A

DATA ACQUISITION & ANALYSIS CODES

The following is a list of the data acquisition and analysis codes that were used in the present project. Files of the SUN and MPAR (Multi-Parameter) type, written in XSYS, were used in chapter three, the performance tests and in chapter four, the efficiency measurements, respectively. The last code in this list is a FORTRAN program used in the analysis of the Time-of-Flight spectra.

I. Data Aquisition Codes

SUN.COM

```
$ PUT 2
$ DMEM ALL
$ AMEM 1 1024 I*4 1D
$ AMEM 2
$ AMEM 3
$ AMEM 10 R*4 1024
$ GATE 1 5
$ GATE 2 5
$ GATE 3 5
$ EVOP SE SUN
$ CLEAR ALL
$ CLEAR FLAGS
$ EXIT
```

SUN.EVL

```
SPEC S1 1
DATA EVSIZ 1
FORMAT F 1 10 1
GET F
INC S1
END
```

SUN.DAP

```
SUN
1
100
INIT
1 28 9 26
1 28 8 26
1 30 10 26
1 1 0 16 1024
1 1 0 26
LAM
1 1 0 2
END
```

MPAR.COM

```
$ PUT 1
$ DMEM ALL
$ AMEM 1 1024 I*4 1D TOF
$ AMEM 2 1024 I*4 1D PSD
$ AMEM 3 1024 I*4 1D ENER
$ AMEM 4 1024 I*4 1D T0F-X
$ AMEM 5 1024 I*4 1D PSD-X
$ AMEM 6 1024 I*4 1D ENER-X
$ AMEM 10 1024 R*4 1D
$ AMEM 11 1024 I*4 1D PSD-G1
$ AMEM 12 1024 I*4 1D PSD-G2
$ AMEM 13 1024 I*4 1D PSD-G3
$ AMEM 14 1024 I*4 1D PSD-G4
$ AMEM 15 1024 I*4 1D PSD-G5
$ AMEM 16 1024 I*4 1D PSD-G6
$ AMEM 17 1024 I*4 1D PSD-G7
$ AMEM 18 1024 I*4 1D PSD-G8
$ AMEM 19 1024 I*4 1D PSD-G9
$ AMEM 20 1024 I*4 1D PSD-G10
```

```
$ GATE NEW
$ GATE 1 2
$ GATE 2 2
$ GATE 3 2
$ GATE 4 2
$ GATE 5 2
$ GATE 6 2
$ EVOP SE MPAR
$ CL ALL
$ EXIT
```

MPAR.EVL

```
OPTION DUMP
SPEC TOF 1
SPEC PSD 2
SPEC ENER 3
SPEC GAT1 11
SPEC GAT2 12
SPEC GAT3 13
SPEC GAT4 14
SPEC GAT5 15
SPEC GAT6 16
SPEC GAT7 17
SPEC GAT8 18
SPEC GAT9 19
SPEC GAT0 20
DATA EVSI 3
GATE G31 3 1
GATE G32 3 2
GATE G33 3 3
GATE G34 3 4
GATE G35 3 5
GATE G36 3 6
GATE G37 3 7
GATE G38 3 8
```

```
GATE G39 3 9
GATE G30  3 10
FORMAT X 1 10 1
FORMAT Y 2 10 1
FORMAT Z  3 10 1
GET X
INC TOF
GET Z
INC ENER
GET Y
INC PSD
GET Z
IF G31
GET Y
INC GAT1
ELSE
ENDIF
GET Z
IF G32
GET Y
INC GAT2
ELSE
ENDIF
GET Z
IF G33
GET Y
INC GAT3
ELSE
ENDIF
GET Z
IF G34
GET Y
INC GAT4
ELSE
ENDIF
GET Z
```

```
IF G35
GET Y
INC GAT5
ELSE
ENDIF
GET Z
IF G36
GET Y
INC GAT6
ELSE
ENDIF
GET Z
IF G37
GET Y
INC GAT8
ELSE
ENDIF
GET Z
IF G39
GET Y
INC GAT9
ELSE
ENDIF
GET Z
IF G30
GET Y
INC GAT0
ELSE
ENDIF
END
```

MPAR.DAP

```
MPAR
1
300
```

```
INIT
1 28 9 26
1 28 8 26
1 30 10 26
1 14 0 16 1024
1 15 0 16 1024
1 16 0 16 1024
1 14 0 26
1 15 0 26
1 16 0 26
LAM
1 14 0 2
1 15 0 2
1 16 0 2
END
```

II. TOF Spectra Analysis Code

```
      IMPLICIT REAL*8 (A-H,O-Z)
      DIMENSION ENER(1024), ICHAN(1024), VEL(1024)
      DIMENSION ISPEC(1024), CFSPEC(1024), EFF(1024)
      REAL*8 MC2
      MC2=939.505
      C=0.2997925
      IGAMPK=876
      TCALB=0.104
      FLP=0.976
C
C     INITIALIZATION
C
      DO 1 J=1,1024
      CFSPEC(J)=0
      ISPEC(J)=0
      EFF(J)=0
      ENER(J)=0
      LIMITS(1,J)=0
```

```
      LIMITS(2,J)=0
      ICHAN(J)=0
      VEL(J)=0
 1    CONTINUE
C
C     READ COUNTS IN EACH TOF CHANNEL AND GENERATE ROTATED
C     TOF SPECTRUM
C
      READ(11,*) IDATA
      DO 7 K=1,1024
      MM=1024-K
 7    IROTSPEC(MM) = IDATA(K)
C
C     GENERATE THE ENERGY DISTRIBUTION FOR THE 252CF SOURCE
C
      DO 10 I=1,1024
      DD=I
      ENER(I)=0.025*DD
 10   CFSPEC(I)=DSQRT(ENER(I))*DEXP(-ENER(I)/1.355)
C
C     CALCULATING THE TIME OF ARRIVAL OF GAMMA RAYS,
C     NEUTRONS, NEUTRON VELOCIT AND THEN ENERGY.
C
      IGG=IGAMPK-1
      DO 878 K=1,IGG
      DDT=IGAMPK-K
      DELT=(DDT*TCALB)+(FLP/C)
      VEL(K)=FLP/DELT
      BETA=VEL(K)/C
      IF (BETA.GE.1.)  GOTO 878
      IF (BETA.GT.0.1) GOTO 870
      CHEN(K)=0.5*(MC2/C**2)*VEL(K)**2
      IF (CHEN(K).GT.99.) CHEN(K)=99.
      GOTO 878
 870  CHEN(K)=MC2*(DSQRT(1./(1-BETA**2))-1.)
      IF (CHEN(K).GT.99.) CHEN(K)=99.
```

```
 878  CONTINUE

C
C     GENERATE THE ENERGY SPECTRUM FROM THE TOF SPECTRUM
C
      DO 900 K=1,1024
      DSTEP=0.01
      EN=DSTEP*K
      ENER(K)=EN
      ISPEC(K)=0
      IF (EN.LT.0.6) GOTO 900
      DO 555 LI=1,1024
      IF (CHEN(LI).LT.EN) GOTO 555
      ICHAN(K)=LI
      GOTO 900
 555  CONTINUE
 900  CONTINUE
C
C     SUBTRACTING  CONSTANT  BACKGROUND
C
      IBK=2
      DO 1234 M=1,1024
      IF (IROTSPEC(M).EQ.0) GOTO 1234
      IROTSPEC(M)=IROTSPEC(M)-IBK
 1234 CONTINUE
C
C     SETTING  ENERGY  GATES  ON  THE  ENERGY  SPECTRUM  AND
C     SUBTRACTING  THE  TIME  DEPENDENT  BACKGROUND  AND
C     GENERATING THE INTEGRAL SPECTRUM
C
      DO 1200 K=1,1020
      LIMITS(1,K)=ICHAN(K)
      LIMITS(2,K)=ICHAN(K+1)-1
      LL=LIMITS(1,K)
      LU=LIMITS(2,K)
      IF(LU.LT.LL) LL=LU
```

```
      IF(LU.GT.1024) GOTO 1111
      IBG11=20
      IBG13=11
      IBG=IBG13*(LU-LL+1)
      DO 1111 N=LL,LU
      ISPEC(K)=IROTSPEC(N)+ISPEC(K)
 1111 CONTINUE
      IF (ISPEC(K).LT.0) ISPEC(K)=0
      DT=ISPEC
C
C     EFFICIENCY IS FOUN BY DIVIDING THE EXPERIMENTALLY
C     GENERATED SPECTRUM BY THE STANDARD 252CF SPECTRUM
C
      EFF(K)=DT/CFSPEC(K)
 1200 CONTINUE
      WRITE(15,55)(I,ENER(I),ICHAN(I),LIMITS(1,I),LIMITS(2,I),ISPEC(I),
      C IROTSPEC(I),I=1,1024)
 55   FORMAT (3(I6,F8.3,5I5,2X))
      WRITE(9,*) ISPEC
      WRITE(9,*) EFF
      END
```

NOMENCLATURE

ADC	Analog-to-Digital Convertor
CFD	Constant Fraction Discriminator
DDL	Double Delay Linear Amplifier
dE/dx	Specific Energy Loss
DGG	Dual Gate Generator
E_R	Energy of Recoiling Particle
E_γ	Energy of the Incident Gamma Ray
E_e	Energy of the Compton Electron
E_c	Maximum Energy of the Compton Electron
E_h	Energy at Half-Height the Compton Edge
E_m	Energy at the Maximum of the Compton Edge
FWHM	Full Width at Half Maximum
GDG	Gate & Delay Generator
η	Neutron Detection Efficiency
LAM	Look-at-Me Signal
LG	Light guide
LGS	Linear and Gate Stretcher
LFO	Linear Fan-Out
MBD	Micro-Programmable Branch Drive
PSD	Pulse Shape Discrimination
SCA	Single Channel Analyzer
TAC	Time-to-Amplitude Converter
t_n	Time of Arrival of Neutrons
t_γ	Time of Arrival of Gamma Rays
TOF	Time-of-Flight
UC	Universal Coincidence

REFERENCES

1. A.A. Naqvi, H.Al-Juwair, and K.Gul, Nucl. Inst. and Meth. A306(1991)267

2. R.B. Galloway and D.G. Vass, Nucl. Instr. and Meth. 83 (1970) 35

3. J. F. Knoll' Radiation Detection and Measuremets' New York, Wiley 1979

4. T.A. Love, R.T. Santaro, R.W. Peelle, and N.W. Hill, Rev. Sci. Inst. 39(1968)541

5. D.G. Crabb, J.G. McEwen, E.G. Auld and A. Longsford, Nucl. Instr. and Meth. 48 (1967) 87

6. M. Drosg, Nucl. Instr. and Meth. 105 (1972) 573

7. K. Gul, A.A. Naqvi and H.Al-Juwair, Nucl. Instr. and Meth. A278(1989) 470

8. H.Klien,(PTB) Contribution to the "XII. International Symp. on Nuclear Physics" in Gaubig (1982)

9. H.Marten and D. Seeliger, Nucl. Sci. and Eng. 93(1986)370

10. J. B. Marion and J. L. Fowler, 'Fast Neutron Physics' Interscince Publisher,Inc. New York (1960)

11. N. Tsoulfandis, 'Measurement and Detection of Radiation' McGraw Hill(1983)

12. K. Gul, Nucl. Instr. and Meth. 176 (1980) 549

13. R.Deleo, G. D'trasmo, A. Pantaleo, and G. Russo, Nucl. Instr. and Meth. 119 (1974) 559

14. M.Drosg, D.M.Drake and P. Lisowski, Nucl. Instr. and Meth. 176(1980) 477

15. M.Drosg, Nucl. Sci. and Eng. 67 (1978) 190

16. G. Hout, J. Lachkar, J. Sigaud, Y. Patin and F. Cocu, Nucl. Sci. Eng. 65(1978) 331

17. F. D. Brooks ' Organic Scintillators' in progress in nuclear physics, edited by O.R. Frisch , London, Pergamon Press V.5(1956)

18. D. L. Smith, R. G. Polk, and T. G. Miller, Nucl. Instr. and Meth. 64 (1968) 157

19. J. B. Birks ' The Theory and Practice of Scintillation Counting' Pergamon Press, Oxford 1964

20. R. L. Craum, and D. L. Smith, Nucl. Instr. and Meth. 80 (1970) 239

21. Dietze and Klien, Nucl. Instr. and Meth. 193(1982)549

22. S. Mubarakmand and M. Anwar, Nucl. Instr. and Meth. 93(1971)

23. R. Bottger, H. J. Brade, M. Cosack, G.Dietze, R. Jahr, H. Klein, H. Scholermann, and B. R. L. Siebert, Conribution to the International Conference on "Nuclear Data for Science and Technology" (1982) Antwerp

24. Scintillator Catalogue, Nuclear Interprises Ltd., Edinburgh, Scotland

25. H. Schoolermann and H. Klein, Nucl. Instr. and Meth. 169 (1980) 25

26. G. Dietze, IEEE Trans. Nucl. Sci. NS-26 (1979) 398.

27. H. Al-Juwair and R.E. Abdel-Aal, IEEE Trans. Nucl. Sci. 36(1989) 611

28. R.E. Abdel-Aal and H. Al-Juwair, IEEE Trans. Nucl. Sci. 36(1989) 692

29. J. A. Harvey, and N. W. Hill, Nucl. Instr. and Meth. 162 (1979) 507

30. S. Sanyal, S. C. Pancholi and S. L. Gupta, Nucl. Instr. and Meth. 136 (1976) 157

31. A. C. Melissions 'Experiments in Modern Physics' Academic press, New York 1966

32. J.R.M. Annand, R.W. Finlay and M.A. Polster, Nucl. Instr. and Meth. A234(1985) 483

33. A.A.Naqvi, H. Al-Juwair and K. Gul, AJSI (to be published)

34. S. Bose, M. B. Chatterjee, B. K. Sinha and R. Bhattacharyya, Nucl. Instr. and Meth. A270 (1988) 487

35. D. W. Glasgow, D. E. Velkley, J. D. Brandenberger, and M. T. McEllistrem, Nucl. Instr. and Meth. 114 (1974) 535

36. R. A. Winyard, J. E. Lutkin and G. W. McBeth, Nucl. Instr. and Meth. 95(1971)141

37. P. Sperr. et al. Nucl. Instr. and Meth. 116 (1974) 55

38. R. Bottger, H.Klien, A. Chalupka, and B. Strohmair, Contribution to the International Conference on "Nuclear Data for Science and Technology" (1982) Antwerp

39. R.A. Cecil, B.D. Anderson, and R. Madey, Nucl. Instr. and Meth. 161(1979)439

40. R. Batchelor, W. B. Gilboy, J.B. Parker, J.H. Towle, Nucl. Instr. and Meth. 13 (1961) 70